INTERNATIONAL JOURNAL FOR NUMERICAL METHODS IN ENGINEERING
Int. J. Numer. Meth. Engng 2013; **93**:1255–1285
Published online 4 December 2012 in Wiley Online Library (wileyonlinelibrary.com). DOI: 10.1002/nme.4426

Matching boundary conditions for lattice dynamics

X. Wang[1] and S. Tang[2,*,†]

[1]*Center for Combustion Energy and Department of Thermal Engineering, Tsinghua University, Beijing 100084, China*
[2]*HEDPS, CAPT and LTCS, College of Engineering, Peking University, Beijing 100871, China*

SUMMARY

We design a class of accurate and efficient absorbing boundary conditions for molecular dynamics simulations of crystalline solids. In one space dimension, the proposed matching boundary conditions take the form of a linear constraint of displacement and velocity at atoms near the boundary, where the coefficients are determined by matching the dispersion relation with a minimal number of atoms involved. Bearing the nice features of compactness, locality, and high efficiency, the matching boundary conditions are then extended to treat the out-of-plane wave problems in the square lattice. We construct multidirectional absorbing boundary conditions via operator multiplications. Reflection coefficient analysis and numerical studies verify their effectiveness for spurious reflection suppression in all directions. Compact and local in both space and time, they are directly applicable to nonlinear lattices and multiscale simulations. Copyright © 2012 John Wiley & Sons, Ltd.

Received 22 March 2012; Revised 19 June 2012; Accepted 11 September 2012

KEY WORDS: artificial boundary condition; molecular dynamics; multiscale computation; dispersion relation; reflection coefficient

1. INTRODUCTION

In this paper, we are concerned with the design of artificial boundary conditions (ABCs) for molecular dynamics (MD) simulations in a reduced domain of crystalline solids.

Molecular dynamics simulation methods are widely implemented to investigate mechanical behaviors of materials. While retaining high accuracy, it is yet computationally expensive. To push the frontier of physics under the limited computational powers and memory, in many applications, only a small critical part of the problem is computed by detailed MD simulations. The rest part is dropped or represented by a coarse-grained model [1–3]. For such MD simulations, the artificial boundaries need to be treated carefully. Otherwise, large spurious reflections may severely pollute the MD solutions and sometimes even cause numerical instability [4].

For the MD simulations and the coupled atomic-continuum simulations of crystalline solids, many ABCs, also named as absorbing boundary conditions, have been developed. The time history kernel treatment, which mimics the effects of the dropped atomic part, is the first accurate ABC for a harmonic chain [5, 6]. It has been systematically studied and implemented by Liu *et al.* to multiple dimensional lattices under the framework of the bridging scale method [7–14]. This treatment involves a heavy numerical cost in time convolution and requires accurate calculations of the kernel functions, which is not easy in multiple dimensions [15]. In addition, its nonlocality in time reduces the accuracy when it is applied to nonlinear lattices.

As an alternative, local ABCs have been developed. For example, via one-way wave equations, a class of multilayer velocity interfacial conditions (VICs) were designed for the lattice dynamics [16].

*Correspondence to: S. Tang, HEDPS, CAPT and LTCS, College of Engineering, Peking University, Beijing 100871, China.
†E-mail: maotang@pku.edu.cn

Local in both space and time, this kind of boundary treatment is applicable to lattices with large deformation and relatively strong nonlinearity. Meanwhile, stemmed from the well-known paper by Engquist and Majda [17], some kinds of local ABCs were proposed with the basic idea of minimizing the reflection coefficient [18–20]. A simplification in the design was proposed, where minimization is performed with respect to the perfectly absorbed wave numbers, instead of the reflection coefficient functional [21]. Nevertheless, minimization can be costly, particularly when it needs to be frequently performed as for a nonlinear problem. Another issue for the reflection coefficient approach arises when the form of the reflection waves may not be clearly identified around boundary with complex geometry.

Most ABCs designed for lattice dynamics are efficient for one-dimensional monoatomic chains. The efficiency in multiple dimensional cases is much more delicate, where various directional incidences need to be treated. Meanwhile, for the continuous wave propagation in an unbounded domain, which corresponds to the long wave limit case, there are extensive studies on the ABCs [17, 22–26]. They aim at dealing with various directional incidences. When lattice dynamics are under consideration, however, it may not be straightforward to extend these methods because of the discrete features and the dispersion [27–30]. For instance, to treat the discrete waves, the perfectly matched layer method for continuous wave propagation has to be improved and further developed [27–29].

In this paper, we propose a new class of ABCs for accurate MD and multiscale simulations of crystalline solids.

For one-dimensional chains, such a condition is expressed as a linear constraint for the displacement and velocity at atoms near the artificial boundary. The combination coefficients are determined by matching the dispersion relation of the lattice vibrations with a minimal number of atoms involved. We call the proposed compact conditions as matching boundary conditions (MBCs). Our goal is to optimize the spurious reflection suppression (accuracy) and the locality in space and time (computational costs). Several atoms near the boundary usually suffice for accuracy requirements in most applications.

The accuracy and the locality allow us to extend this approach to multiple dimensions. Specifically, we consider out-of-plane wave propagations in the square lattice. We first apply the one-dimensional results to construct unidirectional MBCs via apparent wave propagations. Using the products of MBC operators, we then design multidirectional ABCs. The design procedure is straightforward. Similar to the Higdon ABCs for continuous wave problems [26], the multidirectional MBCs are effective to absorb incident waves in all directions.

The rest of this paper is organized as follows. In Sections 2 and 3, we construct the MBCs for the one-dimensional harmonic chain and the square lattice, respectively. After that, we verify the effectiveness of the proposed boundary conditions by the reflection coefficient analysis in Section 4. Numerical studies in Section 5 demonstrate the effectiveness, with comparisons with other treatments. In Section 6, we apply the proposed boundary conditions to treat an anharmonic chain and a Lennard–Jones chain as well as crack propagation of a Slepyan model for Mode III fracture [31]. Finally, we make some concluding remarks in Section 7.

2. FORMULATION OF THE MATCHING BOUNDARY CONDITIONS: ONE SPACE DIMENSION

We consider an infinite linear monatomic chain with nearest neighboring interactions. The dynamics is governed by Newton's law

$$m_a \ddot{u}_j = k_a(u_{j-1} - 2u_j + u_{j+1}). \tag{1}$$

Here, u_j denotes the displacement of the jth atom, m_a is the mass of the atom, and k_a is the elastic constant between two adjacent atoms. After rescaling time by $\sqrt{m_a/k_a}$, we obtain a dimensionless form

$$\ddot{u}_j = u_{j-1} - 2u_j + u_{j+1}. \tag{2}$$

DOI: 10.1002/nme

Figure 1. The left artificial boundary in the harmonic chain.

The goal of an ABC is to identify the evolution of the atom(s) at the artificial boundary using the information of the interior atoms only, such that the outgoing waves are well absorbed. That is, one aims at mimicking the free wave propagation in the original infinite lattice.

For the left artificial boundary atom in an atomic or a multiscale computation (the 0th atom in Figure 1), we propose the following local boundary condition:

$$\sum_{j=0}^{N} c_j \dot{u}_j - \sum_{j=0}^{N} b_j u_j = 0. \tag{3}$$

The coefficients b_j and c_j are to be determined.

As is well known, the dispersion relation

$$\omega(\xi) = 2\left|\sin\frac{\xi}{2}\right|, \quad \xi \in [-\pi, \pi] \tag{4}$$

relates the frequency ω with the wave number ξ for the sinusoidal wave $u_j = e^{i(\omega t + j\xi)}$. When one-way waves are under consideration, only half of the first Brillouin zone $\xi \in [0, \pi]$ needs to be treated, corresponding to a left-going wave [32–34].

This left-going wave, as is readily shown, does not satisfy (3) for all ξ. In fact, we substitute its form $u_j = e^{i(\omega t + j\xi)}$ to the left-hand side of (3) and define a dispersion matching residual function

$$\Delta(\xi) \equiv i\omega(\xi) \sum_{j=0}^{N} c_j e^{ij\xi} - \sum_{j=0}^{N} b_j e^{ij\xi}, \quad \xi \in [0, \pi]. \tag{5}$$

It measures the inconsistency of the MBC for an exact outgoing monochromatic wave solution of the infinite chain. The dispersion relation is matched at a wave number ξ_s if $\Delta(\xi_s) = 0$. On the other hand, if we consider the left-going wave at the boundary $u_j = e^{i(\omega_b t + j\xi)}$ that exactly satisfies the MBC (3), we may define a boundary characteristic frequency $\omega_b(\xi)$ with

$$i\omega_b(\xi) = \sum_{j=0}^{N} b_j e^{ij\xi} \Big/ \sum_{j=0}^{N} c_j e^{ij\xi}. \tag{6}$$

Then, we relate $\Delta(\xi) = i[\omega(\xi) - \omega_b(\xi)] \sum_{j=0}^{N} c_j e^{ij\xi}$ with the difference between $\omega_b(\xi)$ and $\omega(\xi)$. The main advantage of the residual $\Delta(\xi)$ over $\omega(\xi) - \omega_b(\xi)$ is its linearity in terms of b_j and c_j. As we shall see afterwards, this allows us to determine the coefficients by solving a set of linear algebraic equations.

We propose two ways to construct the algebraic equations. The Taylor-type conditions focus on the long wave limit ($\xi \to 0^+$), and the Taylor–Newton-type conditions deal with additional selected wave numbers as well.

2.1. Taylor type: MBCN

Long waves dominate the energy band in most applications. They also propagate faster than short waves, hence reach the artificial boundaries and induce spurious reflections earlier. Therefore, the long wave limit is a primary concern in designing ABCs.

DOI: 10.1002/nme

For a Taylor-type MBC with N atoms, we require the residual function (5) to satisfy

$$\Delta(\xi) = o(\xi^{2N}). \tag{7}$$

This determines uniquely the coefficients in (3), if we set $c_0 = 1$, noticing the homogeneously linear form of (3). The resulted condition is named as MBCN for short.

More precisely, the Taylor expansions around $\xi = 0$ for the terms in the residual function (5) are

$$i\omega(\xi) = \sum_{n=0}^{\infty} a_n (i\xi)^n, \quad \text{with } a_{2m} = 0,\ a_{2m+1} = \frac{2^{-2m}}{(2m+1)!},\ m = 0, 1, 2, \ldots, \tag{8}$$

and

$$e^{ij\xi} = \sum_{n=0}^{\infty} h_{nj} (i\xi)^n, \quad \text{with } h_{nj} = \frac{j^n}{n!}. \tag{9}$$

Substituting these terms into (7) and separating the terms with the same orders of $(i\xi)$, we obtain the following linear algebraic system of order $(2N + 2)$, where the first row gives $c_0 = 1$:

$$\begin{bmatrix} e_1^T & z^T \\ A_{(2N+1)\times(2N+1)} & H_{(2N+1)\times(N+1)} \quad -H_{(2N+1)\times(N+1)} \end{bmatrix} \begin{bmatrix} C \\ B \end{bmatrix} = \begin{bmatrix} e_1 \\ z \end{bmatrix}, \tag{10}$$

where the column vectors are

$$C = \begin{bmatrix} c_0 \\ c_1 \\ \vdots \\ c_N \end{bmatrix}, \quad B = \begin{bmatrix} b_0 \\ b_1 \\ \vdots \\ b_N \end{bmatrix}, \quad e_1 = \begin{bmatrix} 1 \\ 0 \\ \vdots \\ 0 \end{bmatrix}_{(N+1)\times 1}, \quad z = \begin{bmatrix} 0 \\ 0 \\ \vdots \\ 0 \end{bmatrix}_{(N+1)\times 1}, \tag{11}$$

and the matrices are

$$A = \begin{bmatrix} a_0 & & & \\ a_1 & a_0 & & \\ \vdots & \vdots & \ddots & \\ a_{2N} & a_{2N-1} & \cdots & a_0 \end{bmatrix}, \ H = \begin{bmatrix} h_{00} & h_{01} & \cdots & h_{0N} \\ h_{10} & h_{11} & \cdots & h_{1N} \\ \vdots & \vdots & \cdots & \vdots \\ h_{2N\,0} & h_{2N\,1} & \cdots & h_{2N\,N} \end{bmatrix}. \tag{12}$$

The coefficients $c_0, c_1, \ldots, c_N$ and $b_0, b_1, \ldots, b_N$ are solved from (10).

For example, MBC1 takes $N = 1$. We may approximate the dispersion relation up to $o(\xi^2)$. The matrices are

$$A = \begin{bmatrix} a_0 & & \\ a_1 & a_0 & \\ a_2 & a_1 & a_0 \end{bmatrix}, \quad H = \begin{bmatrix} h_{00} & h_{01} \\ h_{10} & h_{11} \\ h_{20} & h_{21} \end{bmatrix} = \begin{bmatrix} 1 & 1 \\ 0 & 1 \\ 0 & 1/2 \end{bmatrix}. \tag{13}$$

The equation (10) reads

$$\begin{bmatrix} 1 & 0 & 0 & 0 \\ a_0 & a_0 & -1 & -1 \\ a_1 & a_1 + a_0 & 0 & -1 \\ a_2 & a_2 + a_1 + a_0/2 & 0 & -1/2 \end{bmatrix} \begin{bmatrix} c_0 \\ c_1 \\ b_0 \\ b_1 \end{bmatrix} = \begin{bmatrix} 1 \\ 0 \\ 0 \\ 0 \end{bmatrix}. \tag{14}$$

Noticing $a_0 = a_2 = 0$ and $a_1 = 1$, we obtain

$$c_0 = 1,\ c_1 = 1,\ b_0 = -2,\ b_1 = 2. \tag{15}$$

MBC1 then reads

$$\dot{u}_0 + \dot{u}_1 = -2u_0 + 2u_1. \tag{16}$$

The coefficients for MBC1 through MBC6 are listed in Table I.

DOI: 10.1002/nme

Table I. Coefficients for MBCNs

	c_0	c_1	c_2	c_3	c_4	c_5	c_6	b_0	b_1	b_2	b_3	b_4	b_5	b_6
MBC1	1	1						−2	2					
MBC2	1	6	1					−4	0	4				
MBC3	1	15	15	1				−6	−14	14	6			
MBC4	1	28	70	28	1			−8	−48	0	48	8		
MBC5	1	45	210	210	45	1		−10	−110	−132	132	110	10	
MBC6	1	66	495	924	495	66	1	−12	−208	−572	0	572	208	12

2.2. *Taylor–Newton type: MBC$N(0, \xi_2, \ldots, \xi_N)$*

In this approach, the dispersion relation is approximated in the long wave limit up to $o(\xi^2)$. In addition, we enforce complete absorption at other $(N-1)$ selected wave numbers $\xi_2, \ldots, \xi_N$ with $N \geqslant 2$. One may choose these wave numbers according to the specific problem and incidences. Such a Taylor–Newton-type MBC is abbreviated as MBC$N(0, \xi_2, \ldots, \xi_N)$.

At a wave number $\xi_k \neq 0$, the real and imaginary parts of $\Delta(\xi_k) = 0$ give the following requirements:

$$\begin{cases} \omega(\xi_k) \sum_{j=0}^{N} c_j \sin j\xi_k + \sum_{j=0}^{N} b_j \cos j\xi_k = 0, \\ \omega(\xi_k) \sum_{j=0}^{N} c_j \cos j\xi_k - \sum_{j=0}^{N} b_j \sin j\xi_k = 0, \end{cases} \qquad k = 2, \ldots, N. \tag{17}$$

Together with the matching condition at $\xi = 0$, we obtain the following system:

$$\begin{bmatrix} e_1^T & z^T \\ A_{3\times 3} H_{3\times(N+1)} & -H_{3\times(N+1)} \\ W_{RC} & W_{RB} \\ W_{IC} & W_{IB} \end{bmatrix} \begin{bmatrix} C \\ B \end{bmatrix} = \begin{bmatrix} e_1 \\ z \end{bmatrix}, \tag{18}$$

where the column vectors B, C, e_1, and z are the same as (11) and

$$A_{3\times 3} = \begin{bmatrix} a_0 & & \\ a_1 & a_0 & \\ a_2 & a_1 & a_0 \end{bmatrix}, \; H_{3\times(N+1)} = \begin{bmatrix} h_{00} & h_{01} & \cdots & h_{0N} \\ h_{10} & h_{11} & \cdots & h_{1N} \\ h_{20} & h_{21} & \cdots & h_{2N} \end{bmatrix}. \tag{19}$$

The block submatrices W's of size $(N-1) \times (N+1)$ are formed with the following entries corresponding to the real and imaginary parts of $\Delta(\xi_k) = 0$:

$$(W_{RC})_{k-1,j+1} = \omega(\xi_k) \sin(j\xi_k); \;\; (W_{RB})_{k-1,j+1} = \cos(j\xi_k);$$

$$(W_{IC})_{k-1,j+1} = \omega(\xi_k) \cos(j\xi_k); \;\; (W_{IB})_{k-1,j+1} = -\sin(j\xi_k);$$

where $k = 2, \ldots, N$ and $j = 0, \ldots, N$.

For example, the coefficients in MBC2(0,1) may be computed from

$$\begin{bmatrix} 1 & 0 & 0 & 0 & 0 & 0 \\ a_0 & a_0 & a_0 & -1 & -1 & -1 \\ a_1 & a_1 + a_0 & a_1 + 2a_0 & 0 & -1 & -2 \\ a_2 & a_2 + a_1 + a_0/2 & a_2 + 2a_1 + 2a_0 & 0 & -1/2 & -2 \\ 0 & \omega(1)\sin(1) & \omega(1)\sin(2) & 1 & \cos(1) & \cos(2) \\ \omega(1) & \omega(1)\cos(1) & \omega(1)\cos(2) & 0 & -\sin(1) & -\sin(2) \end{bmatrix} \begin{bmatrix} c_0 \\ c_1 \\ c_2 \\ b_0 \\ b_1 \\ b_2 \end{bmatrix} = \begin{bmatrix} 1 \\ 0 \\ 0 \\ 0 \\ 0 \\ 0 \end{bmatrix}. \tag{20}$$

DOI: 10.1002/nme

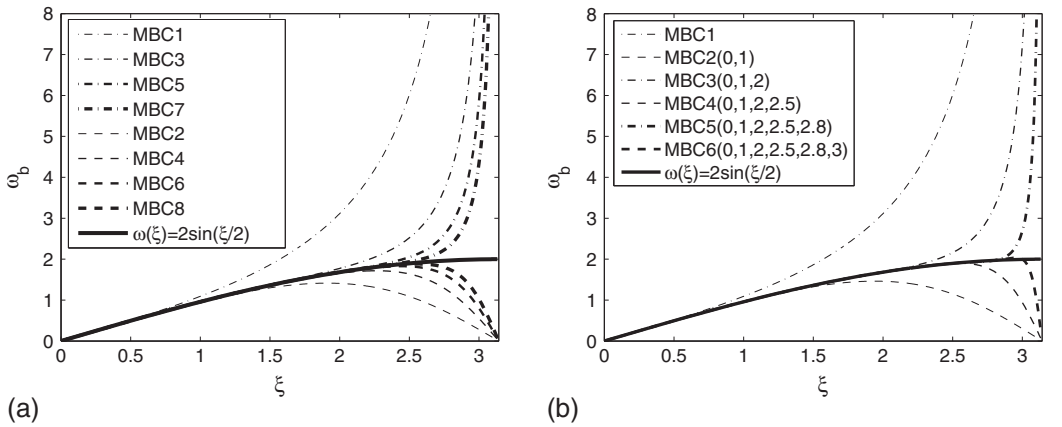

Figure 2. $\omega_b(\xi)$ of matching boundary conditions (MBCs) approximating $\omega(\xi)$: (a) MBCN; (b) MBC$N(0, \xi_2, \ldots, \xi_N)$.

This yields MBC2(0,1)

$$\dot{u}_0 + 5.5103\dot{u}_1 + \dot{u}_2 = -3.7552u_0 + 3.7552u_2. \tag{21}$$

We plot the boundary characteristic frequencies for various MBCs in Figure 2. They are all real and approximate the dispersion relation progressively better as N increases. At a wave number where the dispersion relation is exactly matched by an MBC, the corresponding monochromatic wave of the original infinite chain causes no reflection at the artificial boundary.

Compared with MBCN, which only deals with the long waves near $\xi = 0$, MBC$N(0, \xi_2, \cdots, \xi_N)$ makes a trade-off between long waves and short waves and has a better performance at large wave numbers. Because in most applications long waves dominate, the MBCNs are recommended except for some special cases where wave sources with known wave numbers are important.

Furthermore, because we may express higher order temporal derivatives in terms of displacement or velocity via Newton's law, all linear conditions can be recast into the standard form (3). Some other boundary conditions may also be viewed as degenerate versions of (3), for example, the VICs [16] and the force boundary conditions [35] in Appendix A.

3. FORMULATION OF THE MATCHING BOUNDARY CONDITIONS: TWO SPACE DIMENSIONS

In this section, we design MBCs for the out-of-plane waves in a two-dimensional square lattice shown in Figure 3.

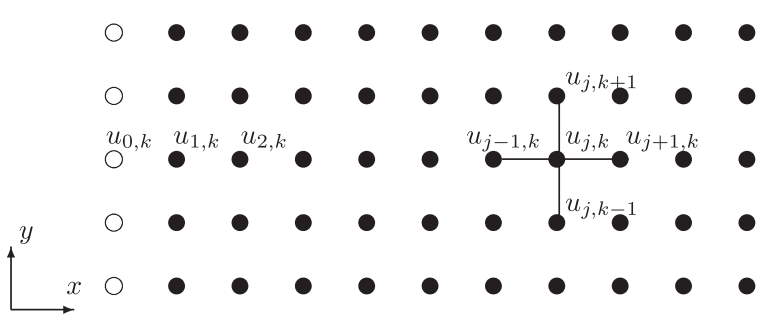

Figure 3. The left artificial boundary (hollow dots) for the square lattice.

DOI: 10.1002/nme

Under the nearest neighboring linear interactions, Newton's law for the out-of-plane displacement of the (j,k)th atom $u_{j,k}$ is given by

$$m_a \ddot{u}_{j,k} = k_a(u_{j-1,k} + u_{j+1,k} + u_{j,k-1} + u_{j,k+1} - 4u_{j,k}). \tag{22}$$

Here, m_a is the mass of the atom and k_a is the elastic constant between two adjacent atoms. The (j,k)th atom locates at $(x_{j,k}, y_{j,k}) = (jh_a, kh_a)$, where h_a is the atomic spacing at rest. Rescaling time by $\sqrt{m_a/k_a}$, we obtain a dimensionless form of

$$\ddot{u}_{j,k} = u_{j-1,k} + u_{j+1,k} + u_{j,k-1} + u_{j,k+1} - 4u_{j,k}. \tag{23}$$

We propose to treat the atomic boundary by operator multiplication of ABCs for several selected directions. Along each direction, a unidirectional MBC is designed with the help of normal apparent wave propagation.

3.1. Unidirectional matching boundary conditions

We consider the left artificial boundary for the square lattice shown in Figure 3. Similar to the one-dimensional case, a general boundary condition may be formulated in the displacement–velocity form of the neighboring interior atoms near the boundary.

Specifically, we propose to design a boundary condition involving atoms only along the normal direction of the boundary, namely the kinetics of a boundary atom $u_{0,k}$ is imposed as

$$\sum_{j=0}^{N} c_j \dot{u}_{j,k} = \sum_{j=0}^{N} b_j u_{j,k}. \tag{24}$$

The dispersion matching residual function is defined as

$$\Delta(\xi_x, \xi_y) \equiv i\omega(\xi_x, \xi_y) \sum_{j=0}^{N} c_j e^{ij\xi_x} - \sum_{j=0}^{N} b_j e^{ij\xi_x}, \quad (\xi_x, \xi_y) \in [0, \pi] \times [-\pi, \pi]. \tag{25}$$

Here, the dispersion relation

$$\omega(\xi_x, \xi_y) = 2\sqrt{\sin^2 \frac{\xi_x}{2} + \sin^2 \frac{\xi_y}{2}}, \tag{26}$$

relates the frequency ω with the wave vector (ξ_x, ξ_y) of a plane wave $u_{j,k}(t) = e^{i(\omega t + j\xi_x + k\xi_y)}$. The smallest periodic unit $[-\pi, \pi] \times [-\pi, \pi]$ is the first Brillouin zone [32–34].

The aforementioned dispersion relation is not differentiable in the long wave limit. Thus, one cannot directly perform the Taylor expansion of the residual function $\Delta(\xi_x, \xi_y)$ to determine the coefficients. Instead, we first consider the normal incidence with $(\xi_x, \xi_y) = (\xi, 0)$. It is reduced to the one-dimensional case and the MBCs presented in the previous subsection apply. For example, MBC1 for the normal incidence reads

$$\dot{u}_{0,k} + \dot{u}_{1,k} = -2u_{0,k} + 2u_{1,k}. \tag{27}$$

To facilitate later discussions, we introduce a shift operator K_x defined by $K_x u_{j,k} = u_{j+1,k}$. Accordingly, we have $(K_x)^l u_{j,k} = u_{j+l,k}$, and $(K_x)^0 = I$ is the identity operator. For instance, the boundary condition (27) is rewritten as

$$\left[Q(K_x) \frac{\mathrm{d}}{\mathrm{d}t} - P(K_x) \right] u_{0,k} = 0. \tag{28}$$

Here, $Q(K_x) = I + K_x$ and $P(K_x) = -2I + 2K_x$.

DOI: 10.1002/nme

To design MBCs for perfectly absorbing plane wave with a given incident angle α in the long wave limit, we require $\Delta(\xi\cos\alpha, \xi\sin\alpha) = o(\xi^2)$. This yields

$$\left[Q(K_x)\frac{\mathrm{d}}{\mathrm{d}t} - aP(K_x)\right]u_{0,k} = 0, \tag{29}$$

where $a = 1/\cos\alpha$ is the normal apparent wave propagation speed. We name it as MBC1-a. In particular, the normal incidence boundary condition MBC1 (27) may be regarded as the shorthand of MBC1-1.

3.2. Multidirectional matching boundary conditions

Following the idea of Higdon for wave propagation in a continuum [26], we construct ABCs by using the products of MBC operators that effectively absorb incident waves at selected directions. This strategy applies to general choices of unidirectional MBCs. Here, we illustrate with MBC1 as an example. That is, we construct the multidirectional MBC

$$\left\{\prod_{j=1}^{M}\left[Q(K_x)\frac{\mathrm{d}}{\mathrm{d}t} - a_j P(K_x)\right]\right\}u_{0,k} = 0, \tag{30}$$

where the artificial normal apparent wave propagation speeds a_j's are chosen as $a_j = 1/\cos\alpha_j$, which control the main absorbing directions with incident angles $\pm\alpha_j$ $(j = 1, \ldots, M)$.

We compute

$$\left(Q\frac{\mathrm{d}}{\mathrm{d}t} - a_1 P\right)\left(Q\frac{\mathrm{d}}{\mathrm{d}t} - a_2 P\right) = QQ\frac{\mathrm{d}^2}{\mathrm{d}t^2} - (a_1 + a_2)QP\frac{\mathrm{d}}{\mathrm{d}t} + a_1 a_2 PP, \tag{31}$$

and

$$QQ = I + 2K_x + K_x^2,\ \ QP = -2I + 2K_x^2,\ \ PP = 4I - 8K_x + 4K_x^2. \tag{32}$$

Letting the operator (31) act on the displacement $u_{0,k}$ of a left boundary atom, we obtain an acceleration boundary condition named as M1M1(a_1, a_2).

$$(\ddot{u}_{0,k} + 2\ddot{u}_{1,k} + \ddot{u}_{2,k}) - 2(a_1 + a_2)(-\dot{u}_{0,k} + \dot{u}_{2,k}) + 4a_1 a_2(u_{0,k} - 2u_{1,k} + u_{2,k}) = 0. \tag{33}$$

Because displacement, velocity, and acceleration (force) of atoms are computed in typical MD simulations, the aforementioned condition is straightforward to implement. Furthermore, we may recast higher order temporal derivatives into displacement and velocity via Newton's law (23) and obtain boundary conditions only involving displacement and velocity.

Indeed, M1M1(a_1, a_2) may be recast into the displacement–velocity form

$$\sum_{j=0}^{5}\sum_{m=-1}^{1} c_{j,m}\dot{u}_{j,k+m} = \sum_{j=0}^{5}\sum_{m=-1}^{1} b_{j,m}u_{j,k+m}, \tag{34}$$

with the following nonzero coefficients.

$$\begin{array}{llll} & b_{1,1} = 1, & b_{2,1} = 2, & b_{3,1} = 1, \\ b_{0,0} = 1, & b_{1,0} = -2 + 4a_1a_2, & b_{2,0} = -6 - 8a_1a_2, & b_{3,0} = -2 + 4a_1a_2, \quad b_{4,0} = 1, \\ & b_{1,-1} = 1, & b_{2,-1} = 2, & b_{3,-1} = 1, \\ & c_{1,0} = -2(a_1 + a_2), & & c_{3,0} = 2(a_1 + a_2). \end{array} \tag{35}$$

DOI: 10.1002/nme

To further improve reflection suppression, one may construct multidirectional MBCs by using more MBC operators. For instance, M1M1M1(a_1, a_2, a_3) in the displacement–velocity form (34) has the following nonzero coefficients:

$$\begin{array}{lll} & b_{1,1} = -b_{4,1} = -2A_1, & b_{2,1} = -b_{3,1} = -2A_1, \\ b_{0,0} = -b_{5,0} = -2A_1, & b_{1,0} = -b_{4,0} = 6A_1 + 8A_3, & b_{2,0} = -b_{3,0} = 8A_1 - 24A_3, \\ & b_{1,-1} = -b_{4,-1} = -2A_1, & b_{2,-1} = -b_{3,-1} = -2A_1, \\ & c_{1,1} = c_{4,1} = 1, & c_{2,1} = c_{3,1} = 3, \\ c_{0,0} = c_{5,0} = 1, & c_{1,0} = c_{4,0} = -1 + 4A_2, & c_{2,0} = c_{3,0} = -8 - 4A_2, \\ & c_{1,-1} = c_{4,-1} = 1, & c_{2,-1} = c_{3,-1} = 3, \end{array} \tag{36}$$

where $A_1 = (a_1 + a_2 + a_3)$, $A_2 = (a_1a_2 + a_2a_3 + a_3a_1)$, and $A_3 = a_1a_2a_3$.

For the purpose of comparisons, we recall that VICs were designed in [16]. The lowest order condition VIC1 is as follows:

$$\dot{u}_{0,k} = -u_{0,k} + u_{1,k}. \tag{37}$$

We may construct multidirectional VICs similarly. In particular, V1V1(a_1, a_2) in the displacement–velocity form (34) is with the following nonzero coefficients:

$$\begin{array}{llll} & b_{1,1} = 1, & & \\ b_{0,0} = 1, & b_{1,0} = -4 + a_1a_2, & b_{2,0} = 1 - 2a_1a_2, & b_{3,0} = a_1a_2, \\ & b_{1,-1} = 1, & & \\ & c_{1,0} = -(a_1 + a_2), & & c_{3,0} = a_1 + a_2. \end{array} \tag{38}$$

V1V1V1(a_1, a_2, a_3) in the displacement–velocity form (34) takes the following nonzero coefficients:

$$\begin{array}{lll} & b_{1,1} = -A_1, & b_{2,1} = A_1, \\ b_{0,0} = -A_1, & b_{1,0} = 5A_1 - A_3, & b_{2,0} = -5A_1 + 3A_3, b_{3,0} = A_1 - 3A_3, b_{4,0} = A_3, \\ & b_{1,-1} = -A_1, & b_{2,-1} = A_1, \\ & c_{1,1} = 1, & \\ c_{0,0} = 1, & c_{1,0} = -4 + A_2, & c_{2,0} = 1 - 2A_2, c_{3,0} = A_2, \\ & c_{1,-1} = 1. & \end{array} \tag{39}$$

In implementations, we take a rectangular atomic domain for computations. Along the boundary parallel to the y-axis, K_y is used to replace K_x in the boundary conditions. At a corner atom in Figure 4, which is the vertex of the atomic domain, we propose the following treatment with the consideration of the symmetry:

$$\left[Q(K_x)\frac{\mathrm{d}}{\mathrm{d}t} - a_x P(K_x)\right]\left[Q(K_y)\frac{\mathrm{d}}{\mathrm{d}t} - a_y P(K_y)\right] u_{0,0} = 0. \tag{40}$$

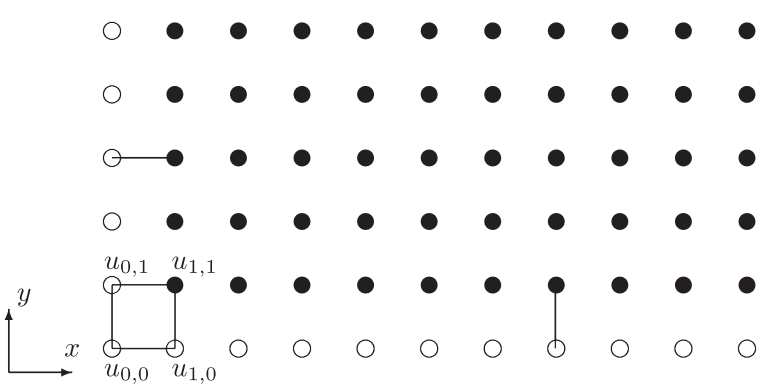

Figure 4. Stencils for the M1M1 at the corner.

DOI: 10.1002/nme

We make a remark here. Compared with the MBCs, the computationally more expensive time history kernel treatment [5–10, 12–14] at corner region needs special treatment, with the kernel functions difficult to evaluate. The corner treatment is delicate and far from well understood in general. Corner reflections appear in most calculations and become prominent if the reflections at other artificial boundary atoms have been well reduced. A recent work made some progress under the framework of the time history kernel treatment [15].

4. EFFECTIVENESS OF MATCHING BOUNDARY CONDITIONS: REFLECTION COEFFICIENT

To illustrate the effectiveness of the proposed MBCs, we first make a reflection coefficient study. Comparisons are made with the VICs.

4.1. One space dimension

In the reflection coefficient analysis, the numerical error is viewed as spurious wave reflection induced at an artificial boundary. We consider a harmonic wave for the left end boundary with a wave number $\xi \in [0, \pi]$,

$$u_j(t) = e^{i[\omega(\xi)t + j\xi]} + Re^{i[\omega(\xi)t - j\xi]}, \tag{41}$$

where the reflection coefficient R measures the amount of the spurious reflection.

Plugging into the MBC (3), we obtain

$$R(\xi) = -\frac{\Delta(\xi)}{\Delta(-\xi)}. \tag{42}$$

Noticing $\omega(-\xi) = \omega(\xi)$, we may find its modulus

$$|R(\xi)| = \left|\frac{\omega(\xi) - \omega_b(\xi)}{\omega(\xi) + \omega_b(\xi)}\right| = (-1)^N \frac{\omega(\xi) - \omega_b(\xi)}{\omega(\xi) + \omega_b(\xi)}. \tag{43}$$

Therefore, for a given wave number, reducing the reflection coefficient is in accordance with approximating the dispersion relation.

We perform the reflection coefficient analysis to MBCN and plot the modulus $|R|$ as a function of ξ in Figure 5. We observe that the MBCNs are effective in the long wave limit. In the log–log plot, the reflection coefficient curves appear as almost straight lines at small wave numbers. Using the L'Hospital rule for MBCN, we have

$$\left.\frac{\mathrm{d}(lg|R|)}{\mathrm{d}(lg\xi)}\right|_{\xi=0+} = \left.\frac{\xi\delta'}{\delta}\right|_{\xi=0+} - \left.\frac{\xi[\omega(\xi) + \omega_b(\xi)]'}{\omega(\xi) + \omega_b(\xi)}\right|_{\xi=0+} = (2N+1) - 1 = 2N,$$

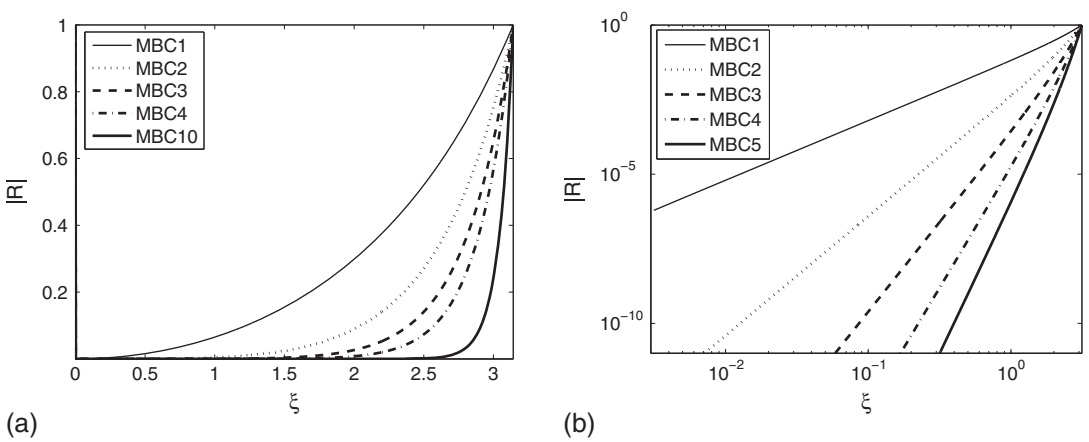

Figure 5. Reflection coefficients of Taylor-type matching boundary conditions (MBCs): (a) linear plots; (b) log–log plots.

DOI: 10.1002/nme

with the frequency difference $\delta(\xi) \equiv \omega(\xi) - \omega_b(\xi) \sim \xi^{2N+1}$. As the order of the MBC increases, the reflection coefficient reduces over the whole range of wave numbers. Furthermore, we remark that the modulus of the reflection coefficient is 1 at $\xi = \pi$, which is a natural limitation. Because the group velocity is zero at this wave number, reflection suppression in numerical simulations is not much influenced.

Next, we perform the reflection coefficient analysis to the Taylor–Newton-type MBCs. Please see Figure 6. The reflection reduction for short waves is effective, as the dispersion relation is matched at more wave numbers. The perfect absorption at the selected wave numbers is manifested in the logarithmic subplot (b) by the downward spikes. At small wave numbers, all the curves are with the same slope 2 because these conditions have the same second-order accuracy there.

For most simulations where long waves dominate, a Taylor-type MBC with two to four neighboring atoms turns out to be sufficient. Only for special cases where very short waves are important, the Taylor–Newton-type conditions are preferred.

Now we make comparisons with some existing ABCs, namely the single-layer and the multilayer VICs (sVICs and mVICs for short). In Figure 7, we observe that higher order sVICs improve absorption only at small wave numbers (about $\xi < 1$), yet they are worse at large wave numbers. The condition sVIC6 even has reflection coefficient bigger than 1, which may lead to instability in numerical computations. Meanwhile, mVIC6 improves absorption over the whole range of wave

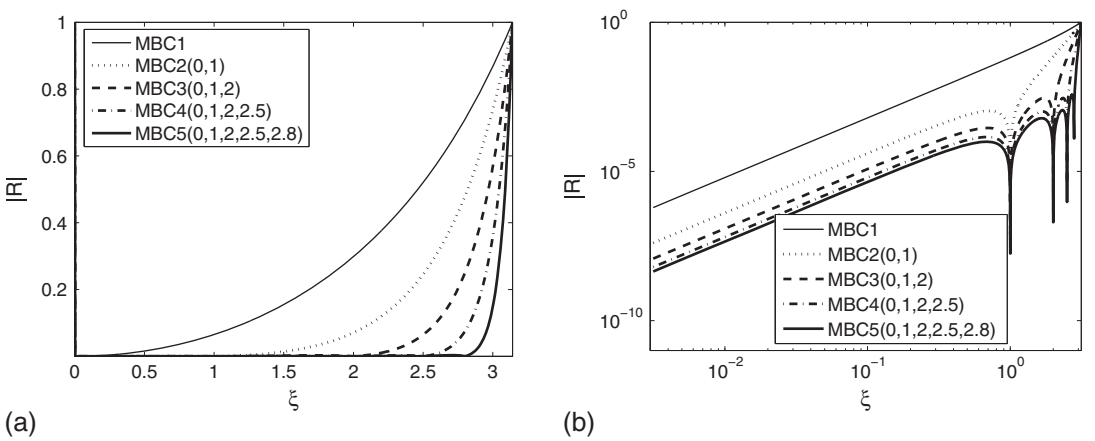

Figure 6. Reflection coefficients of Taylor–Newton-type matching boundary conditions (MBCs): (a) linear plots; (b) log–log plots.

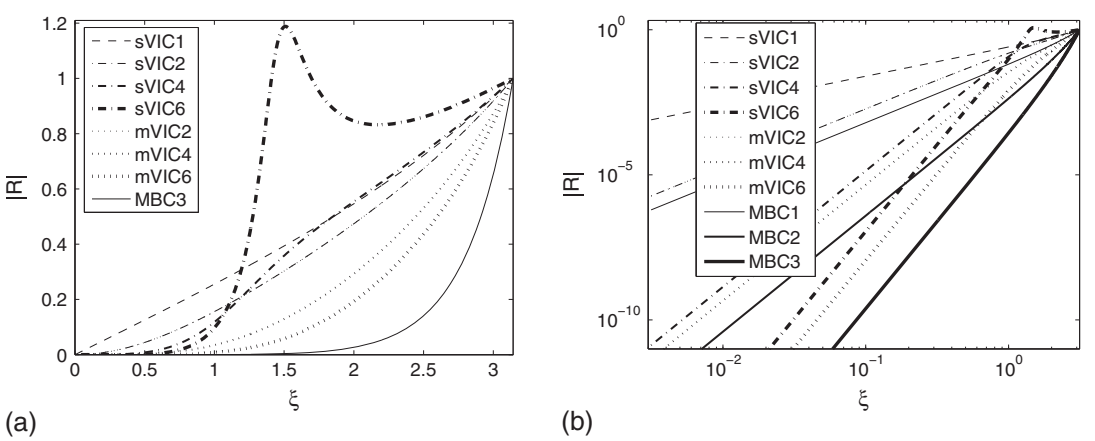

Figure 7. Reflection coefficients of single-layer velocity interfacial conditions (sVICs) and multilayer velocity interfacial conditions (mVICs) compared with matching boundary conditions (MBCs): (a) linear plots; (b) log–log plots.

DOI: 10.1002/nme

numbers. With the same sixth order accuracy at the long wave limit, MBC3 improves much more significantly even at small wave numbers, as shown in the log–log subplot (b). In addition, whereas sVIC6 and mVIC6 involve seven atoms, MBC3 involves only four atoms and is more compact.

The reflection coefficient analysis clearly reveals the effectiveness of the matching dispersion relation approach.

4.2. Two space dimensions

For the square lattice, multidirectional MBCs are further constructed by operator multiplication. We verify the effectiveness of MBCs by the reflection coefficient analysis.

For a characteristic monochromatic incidence with wave number $\xi \in [0, \pi]$ and incident angle $\theta \in [0°, 90°]$, its stationary reflection is also time-harmonic with the same frequency and wave number. Substituting the full wave field

$$u_{j,k}(t) = e^{i[\omega(\xi\cos\theta,\xi\sin\theta)t+j\xi\cos\theta+k\xi\sin\theta]} + Re^{i[\omega(-\xi\cos\theta,\xi\sin\theta)t-j\xi\cos\theta+k\xi\sin\theta]} \tag{44}$$

into the unidirectional MBC (24), we have the reflection coefficient

$$R(\xi,\theta) = -\frac{\Delta(\xi\cos\theta,\xi\sin\theta)}{\Delta(-\xi\cos\theta,\xi\sin\theta)}. \tag{45}$$

The reflection coefficients of VIC1 and MBC1 are depicted in Figure 8 (a.1) and (b.1), respectively. Both are zero at $(\xi,\theta) = (0,0)$, indicating perfect absorption for normal incidence in the long wave limit. The reflection coefficient is smaller with MBC1 over the whole range of wave numbers, demonstrating it suppresses reflections better than VIC1.

Selecting a different angle for full absorption, we propose VIC1-$\sqrt{2}$ and MBC1-$\sqrt{2}$. See Figure 8 (a.2) and (b.2). Full absorption is obtained in the long wave limit at the incident angle 45°. Again, MBC1 has smaller reflections over the whole range of wave numbers.

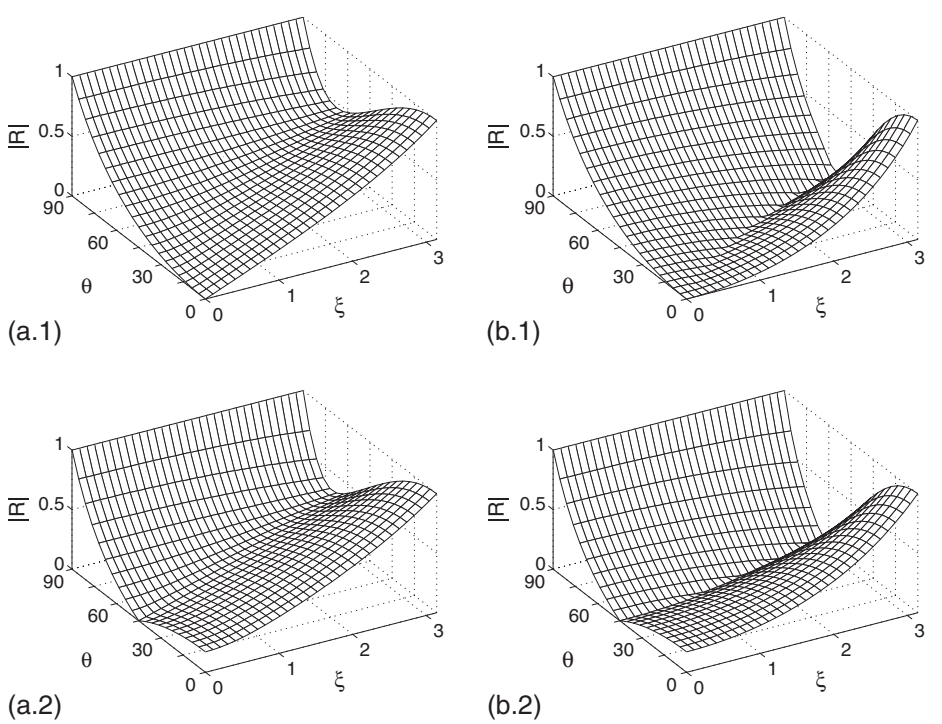

Figure 8. Reflection coefficients of (a.1) VIC1, (b.1) MBC1, (a.2) VIC1-$\sqrt{2}$, and (b.2) MBC1-$\sqrt{2}$. Here, ξ and θ are the wave number and the incident angle (in degree) of a monochromatic incidence wave.

DOI: 10.1002/nme

For the multidirectional MBC (30), we may prove that the reflection coefficient

$$|R(\xi,\theta)| = \prod_{j=1}^{M} |R_j(\xi,\theta)|, \tag{46}$$

where R_j is the reflection coefficient of the unidirectional MBC $\left[Q_j(K_x)\frac{\mathrm{d}}{\mathrm{d}t} - a_j P_j(K_x)\right] u_{0,k} = 0$. In particular, the boundary condition (30) perfectly absorbs waves with incident angles α_j ($j = 1, 2, \ldots, M$) in the long wave limit. For incident waves in other directions or with other wave numbers, the reflection is also efficiently reduced as seen from the multiplication form (46).

In Figure 9, we plot the reflection coefficients for M1M1$\left(1, \sqrt{2}\right)$ and M1M1M1$\left(1, \sqrt{2}, 2\right)$. For M1M1$\left(1, \sqrt{2}\right)$, perfect absorption is reached in the long wave limit for both $\theta = 0°$ and $\theta = 45°$. It is fairly small for most wave vectors with the incident angle not close to 90°. With M1M1M1$\left(1, \sqrt{2}, 2\right)$, perfect absorption is reached also at $\theta = 60°$. The range of a small reflection coefficient is even wider. With reflection coefficients as the products of the reflection coefficients of the corresponding operator factor MBCs, these multidirectional MBCs are much more effective in reflection suppression than unidirectional MBCs.

The effectiveness of an operator multiplication ABC depends on the effectiveness of the corresponding operator factor MBCs. As MBC1 is much effective than VIC1 for reflection suppression, the multidirectional ABCs based on MBC1 are far more effective than those based on VIC1. As shown in Figure 10, MBC1 is even better than V1V1(1,1.4) for normal incident waves.

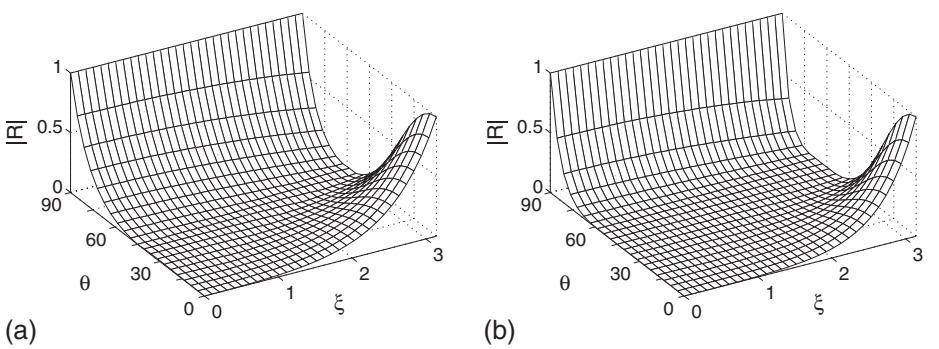

Figure 9. Reflection coefficients of (a) M1M1$\left(1, \sqrt{2}\right)$ and (b) M1M1M1$\left(1, \sqrt{2}, 2\right)$.

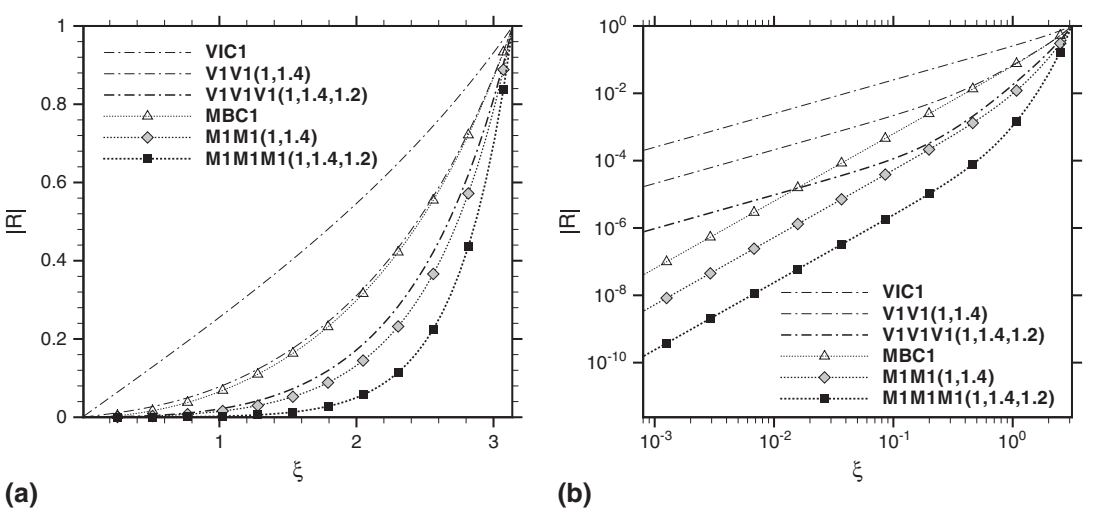

Figure 10. Reflection coefficients for normal incidences: (a) linear plots; (b) log–log plots.

DOI: 10.1002/nme

The aforementioned reflection coefficient analysis clearly demonstrates the effectiveness of reflection suppression with the proposed absorbing boundary conditions.

5. EFFECTIVENESS OF MATCHING BOUNDARY CONDITIONS: NUMERICAL TESTS

In this section, we present some numerical tests to further elaborate the previous analysis.

5.1. One space dimension

We consider a segment of 61 atoms of the infinite harmonic chain, numbered from −30 to 30. The proposed MBCs are imposed on the artificial boundaries, that is, the ±30th atoms.

To manifest the nice features of the MBCs, numerical comparisons are performed against some aforementioned boundary treatments, including sVICs, mVIC4, and the time history kernel treatment.

5.1.1. Numerical implementation. For time integration of Newton's law, a speed Verlet algorithm is adopted.

$$\begin{cases} u_j^{n+1} = u_j^n + \dot{u}_j^n \Delta t + f_j^n \dfrac{(\Delta t)^2}{2}, \\ \dot{u}_j^{n+1} = \dot{u}_j^n + \dfrac{\Delta t}{2}\left(f_j^n + f_j^{n+1}\right), \end{cases} \tag{47}$$

with a time step size $\Delta t = 1/64$. u_j^n is the approximate solution of $u_j(n\Delta t)$.

For the interior atoms ($-29 \leqslant j \leqslant 29$), the force is computed from

$$f_j^n = u_{j-1}^n - 2u_j^n + u_{j+1}^n. \tag{48}$$

With an MBC, the displacement of boundary atoms is updated by

$$u_J^{n+1} = u_J^n + \left(\dot{u}_J^n + \dot{u}_J^{n+1}\right)\frac{\Delta t}{2}, J = \pm 30, \tag{49}$$

where the velocity of boundary atoms is computed from (3). For example, MBC1 at the left boundary reads

$$\dot{u}_{-30}^{n+1} = -2u_{-30}^n + 2u_{-29}^n - \dot{u}_{-29}^n. \tag{50}$$

With sVICs or mVIC4, the boundary atoms are treated similarly. For mVIC4, the innermost layer condition is implemented at the ±30th atoms, and the kinematics of the ±31st and the ±32nd atoms are computed by the velocity conditions.

To make comparison, the exact solution $u_j^{\text{exact}}(t)$ is obtained by simulating a chain long enough such that the boundary effects are negligible because of the finite propagation speeds of the lattice waves.

5.1.2. Numerical results. We take the following initial conditions:

$$u_j(0) = \begin{cases} e^{-j^2/10}, & |j| < 20, \\ 0, & |j| \geqslant 20, \end{cases} \qquad \dot{u}_j(0) = 0. \tag{51}$$

The numerical solutions with sVIC1, sVIC2, and MBC1 are displayed in Figure 11. The wave profile evolves in several stages. For $t < 20$, the initial source splits into two humps, propagating to

DOI: 10.1002/nme

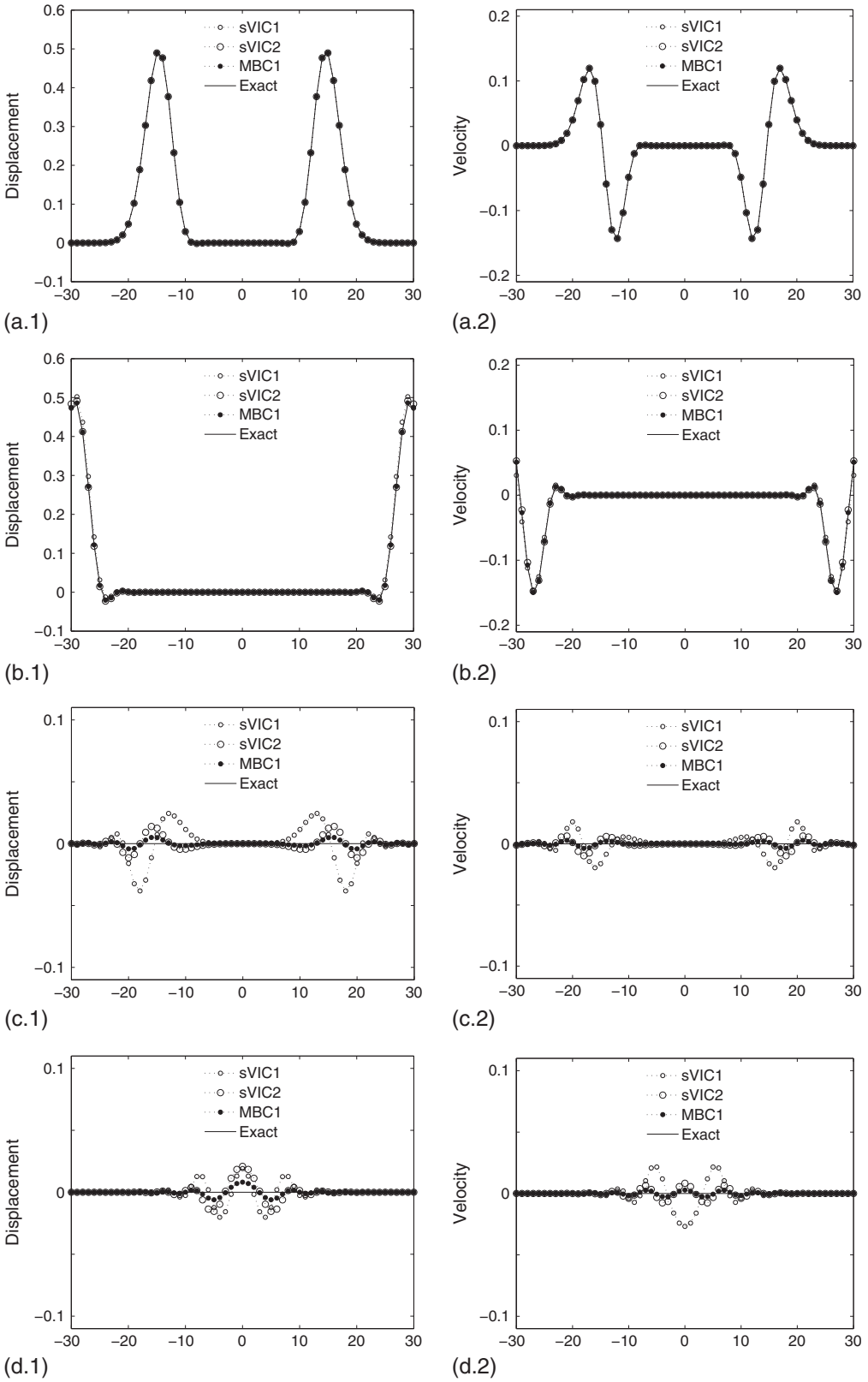

Figure 11. Numerical solutions with sVIC1, sVIC2, and MBC1: (a.1) $u_j(15)$; (a.2) $\dot{u}_j(15)$; (b.1) $u_j(30)$; (b.2) $\dot{u}_j(30)$; (c.1) $u_j(45)$; (c.2) $\dot{u}_j(45)$; (d.1) $u_j(60)$; (d.2) $\dot{u}_j(60)$. The horizontal axes denote the atom numbering.

DOI: 10.1002/nme

two opposite directions. Because of the dispersion, long waves propagate faster, forming the leading humps with large amplitude. Shorter ones are left behind. For $t > 20$, the wavefronts arrive at the boundaries and diminish gradually. With all the three boundary conditions for the segment computations, we observe that the numerical solutions agree very well at $t = 15$ in subplots (a.1) and (a.2). The subplots at $t = 30$ show observable deviations, more readable for the displacement near the boundaries. After this stage, further reflections occur and propagate back to the other end of the segment. In subplots (c.1) and (c.2) at $t = 45$, (d.1) and (d.2) at $t = 60$, the deviations grow to an observable level. MBC1 induces reflection error smaller than sVIC1 and sVIC2.

By increasing N, we involve more atoms in an MBC. In Figure 12, the numerical error with MBC2 at $t = 60$ is about one-tenth of that with MBC1. For comparison, solutions with sVIC4 and mVIC4 of the same fourth-order accuracy in the long wave limit are also displayed. With a numerical cost no bigger than sVIC4 or mVIC4, MBC2 performs much better than them.

The numerical solutions with higher order MBCs at $t = 60$ are shown in Figure 13. The results are significantly improved with increasing N. Noticing the magnitude order of the exact solution, we observe that the reflection errors are very small. Especially the solution with MBC5 is indiscernible from the exact solution.

In summary, we demonstrate the effectiveness of the proposed MBCs with the numerical tests, consistent with the reflection coefficient analysis.

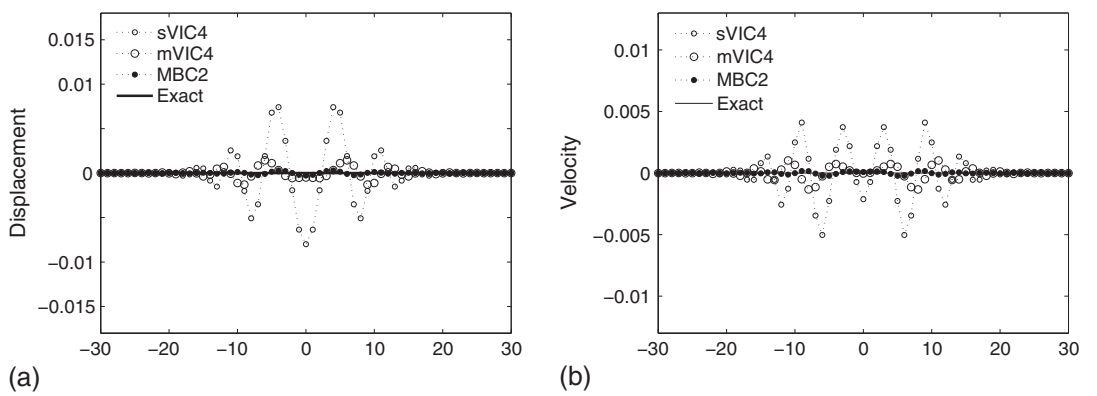

Figure 12. Numerical solutions with sVIC4, mVIC4, and MBC2 at $t = 60$: (a) displacement; (b) velocity. The horizontal axes denote the atom numbering.

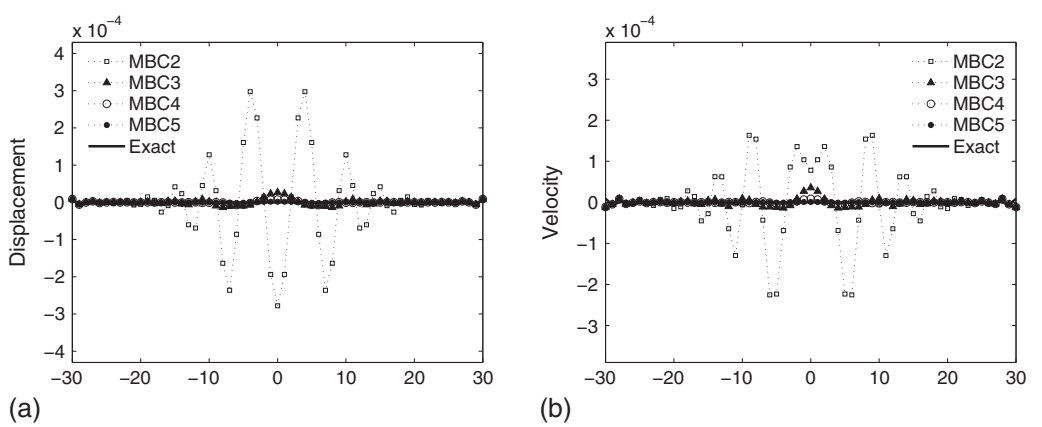

Figure 13. Numerical solutions with matching boundary conditions (MBCs) at $t = 60$: (a) displacement; (b) velocity. The horizontal axes denote the atom numbering.

DOI: 10.1002/nme

5.1.3. Comparison with the time history kernel treatment. To make further comparison, we compute the same numerical test problem with the time history kernel treatment, which is viewed as the most accurate ABC for the harmonic lattice.

The time history kernel treatment constructs the displacement of the boundary atom by using the displacement history of its interior neighboring atom(s). For the one-dimensional monoatomic chain (2), at the 0th atom as the left boundary, it reads

$$u_0(t) = \int_{t-T_c}^{t} \theta(t-\tau) u_1(\tau) \mathrm{d}\tau, \tag{52}$$

with the kernel function

$$\theta(t) = \frac{2J_2(2t)}{t}. \tag{53}$$

Here, J_2 is the Bessel function of the first kind, and T_c is the cutoff time.

We denote it as THK-T_c for short. For instance, THK-50 stands for the time history kernel treatment with $T_c = 50$. Theoretically speaking, THK-T_c reproduces the exact solution within the cutoff time $t \leqslant T_c$. With increasing cutoff time T_c, the reflection error is reduced and delayed.

To implement the time history kernel condition at the left boundary atom numbered -30, we take a cutoff time $T_c = n_H \triangle t$ and compute the convolution by

$$u_{-30}^n = \sum_{k=0}^{n_H} \alpha_k u_{-29}^{n-k}, \tag{54}$$

where α_k's are the coefficients in the numerical integration with the Simpson's rule.

For the time history kernel treatment, considerable computations are involved in the numerical convolution. For a chain of n_A atoms, the interior chain computation costs $O(n_T n_A)$ with n_T the total time steps for simulation. The boundary condition, on the other hand, costs $O(n_T n_H)$. In contrast, the local boundary treatments cost only $O(n_T)$. In a typical multiscale computation, one has $n_H > n_A$. For instance, we consider the previous chain with $n_A = 61$ and take $T_c = 100$ with $\triangle T = 1/64$. Consequently, $n_H = 6400$, much bigger than n_A. Most computations are therefore spent on the time history kernel treatment. In contrast, all the aforementioned local boundary treatments have negligible computational costs.

The numerical solution with THK-50 is displayed in Figure 14. The solution is very accurate at time $t = 60$ after the waves have reached the boundaries. At $t = 90 = T_c + 40$ and $t = 110 = T_c + 60$, however, the reflections are not small. In subplots (d.1) and (d.2), it is obvious that there is a shift in displacement of all atoms due to the reflection of the long waves.

To quantify the reflection, we define the total energy in the computed segment.

$$E(t) = \frac{1}{2} \sum_{j=-30}^{29} (u_{j+1} - u_j)^2 + \frac{1}{2} \sum_{j=-30}^{30} \dot{u}_j^2.$$

The energy evolution, rescaled by the initial energy $E_0 = E(0)$, is plotted in Figure 15. Before the leading humps arrive at the boundaries, the total energy conserves. Computations with MBC4 and MBC5 even correctly capture the energy of magnitude order 10^{-8} at $t = 60$ in Figure 15(a). As shown in the subplot Figure 15(b), the energy evolution with THK-T_c is accurate within the cutoff time T_c. The reflections are delayed and reduced by an increasing T_c. However, despite their larger computing load, the accuracy is still worse than MBC4.

From the aforementioned comparison, we conclude that the proposed MBCs are more efficient than the time history kernel treatment.

DOI: 10.1002/nme

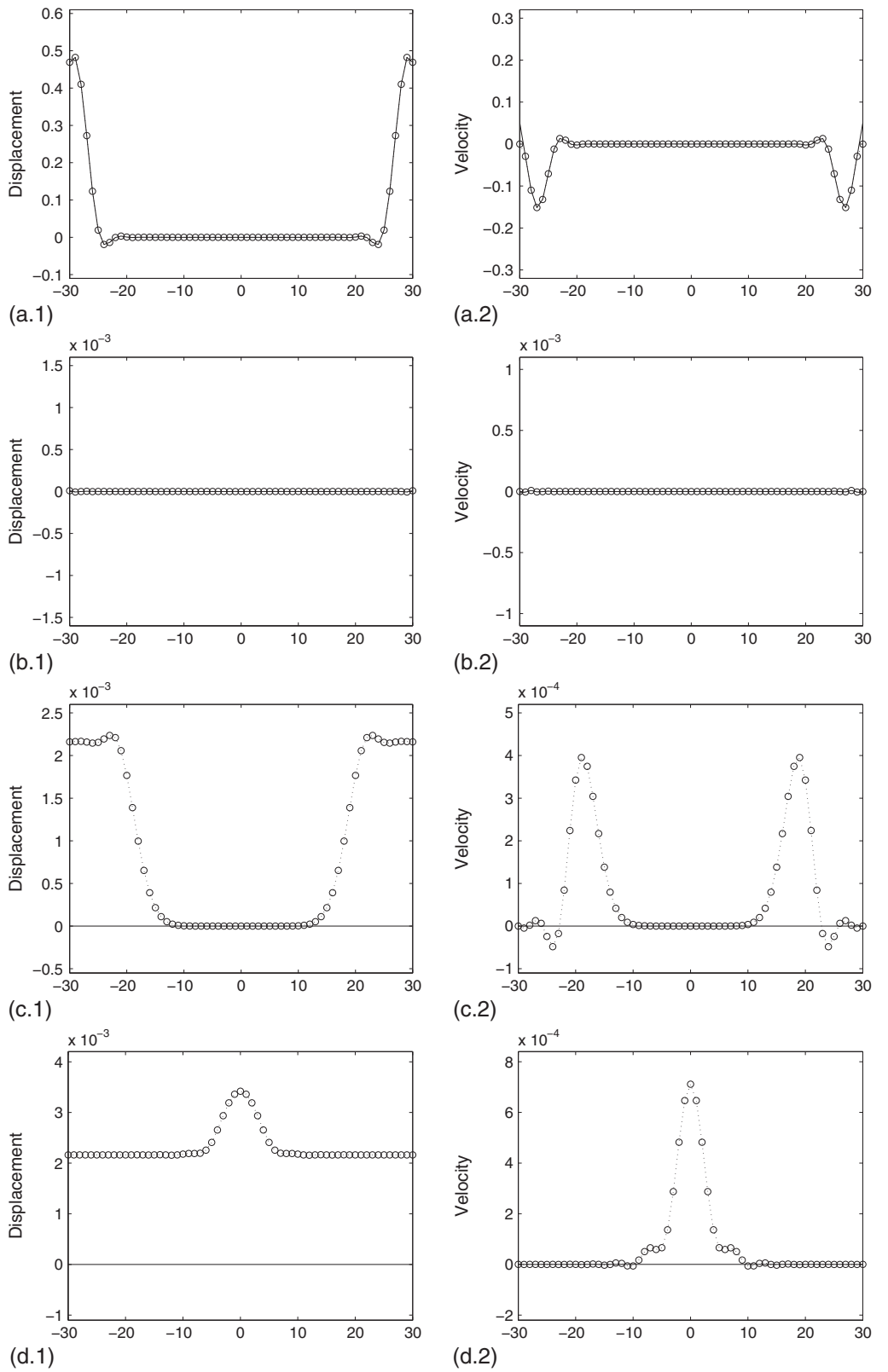

Figure 14. Numerical solution with THK-50: (a.1) $u_j(30)$; (a.2) $\dot{u}_j(30)$; (b.1) $u_j(60)$; (b.2) $\dot{u}_j(60)$; (c.1) $u_j(90)$; (c.2) $\dot{u}_j(90)$; (d.1) $u_j(110)$; (d.2) $\dot{u}_j(110)$. The horizontal axes denote the atom numbering. Solid curves represent the exact solution. Dots represent the solution with THK-50.

DOI: 10.1002/nme

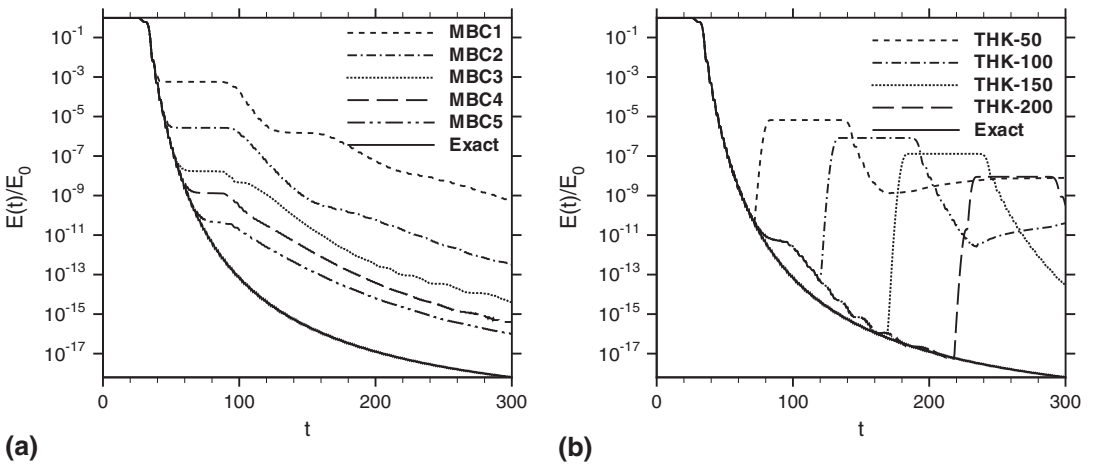

Figure 15. Energy evolution in the segment with (a) matching boundary conditions (MBCs) and (b)THKs.

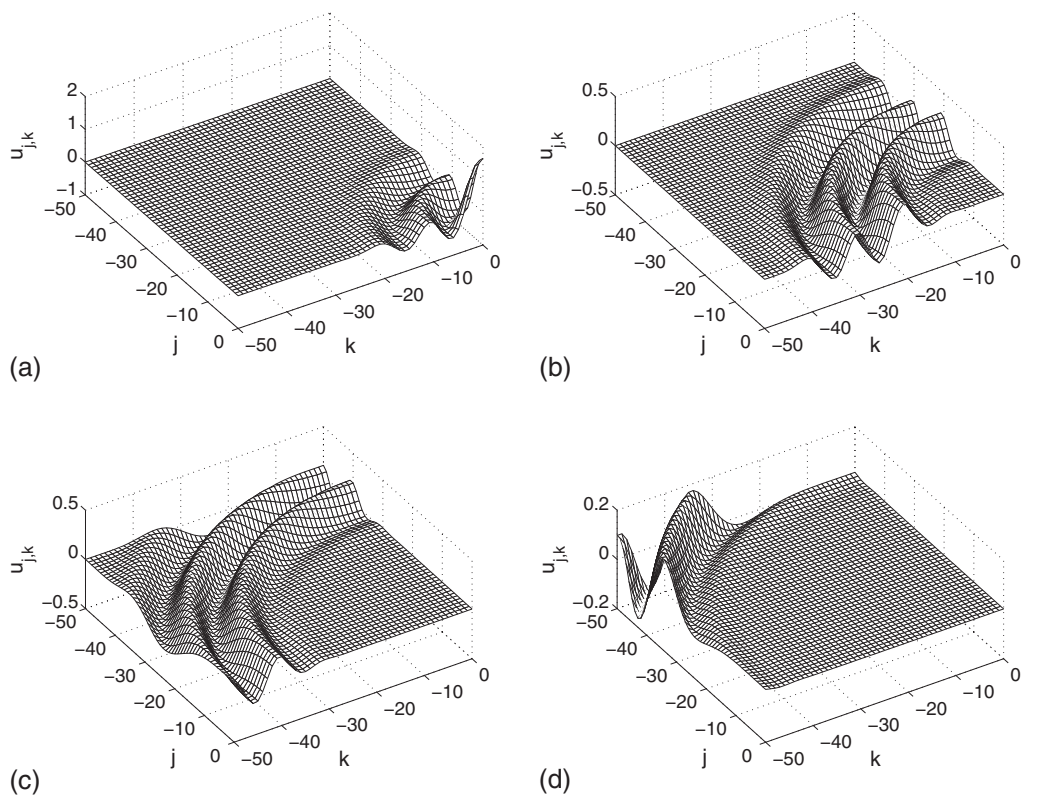

Figure 16. The exact solution (displacement) at (a) $t = 10$, (b) $t = 30$, (c) $t = 50$, and (d) $t = 70$. The test is with the major wave number $\xi_0 = 0.5$. Because of the symmetry, only a quarter of the computing domain is shown.

5.2. Two space dimensions: wave packet tests

We consider a patch of 101×101 atoms of the infinite square lattice, with both indices j and k from -50 to 50. In each simulation, one of the following ABCs are imposed on the four artificial boundaries: MBC1, M1M1(1, 1.4), and M1M1M1(1, 1.2, 1.4). To make comparison, numerical computations with VIC1 and the corresponding operator multiplication conditions (V1V1 and V1V1V1) are performed as well.

DOI: 10.1002/nme

Time integrations are performed in the same way as the one-dimensional chain (47)–(50). We note that for M1M1 in the force form (55), we compute the force from

$$\begin{aligned} f_{-50,k}^{n+1} = &-\left(2f_{-49,k}^{n} + f_{-48,k}^{n}\right) + 2(a_1 + a_2)\left(-\dot{u}_{-50,k}^{n} + \dot{u}_{-48,k}^{n}\right) \\ &- 4a_1a_2\left(u_{-50,k}^{n} - 2u_{-49,k}^{n} + u_{-48,k}^{n}\right), \quad k = -49, \ldots, 49. \end{aligned} \tag{55}$$

Here, we take $a_1 = 1$ and $a_2 = 1.4$. The aforementioned Verlet scheme then gives the velocity and displacement for the left boundary atoms.

To make comparison, the exact solution $u_{j,k}^{\text{exact}}(t)$ is obtained by simulating a patch large enough such that the boundary effects are negligible.

The initial wave packet is centered at the (0,0)th atom.

$$u_{j,k}(0) = \begin{cases} e^{-r^2/100}\left[\cos\left(r\left(\xi_0 - \dfrac{\pi}{40}\right)\right) + \cos\left(r\left(\xi_0 + \dfrac{\pi}{40}\right)\right)\right], |r| < 30, \\ \qquad\qquad\qquad\qquad\qquad\qquad \dot{u}_{j,k}(0) = 0. \\ 0, |r| \geqslant 30, \end{cases}$$

Here, $r^2 = (j-10)^2 + k^2$. The major wave number ξ_0 is set to be 0.5 and 1 in two tests, respectively.

Figure 16 shows the exact solution in the test with $\xi_0 = 0.5$. The wave profile propagates outward and disperses. After reaching the boundaries, waves diminish gradually. Numerical solutions with various ABCs at $t = 70$ are shown in Figure 17. It is observed that MBC1 performs better than VIC1. The M1M1 solution has no visible reflections, much better than the MBC1 solution and the V1V1 solution.

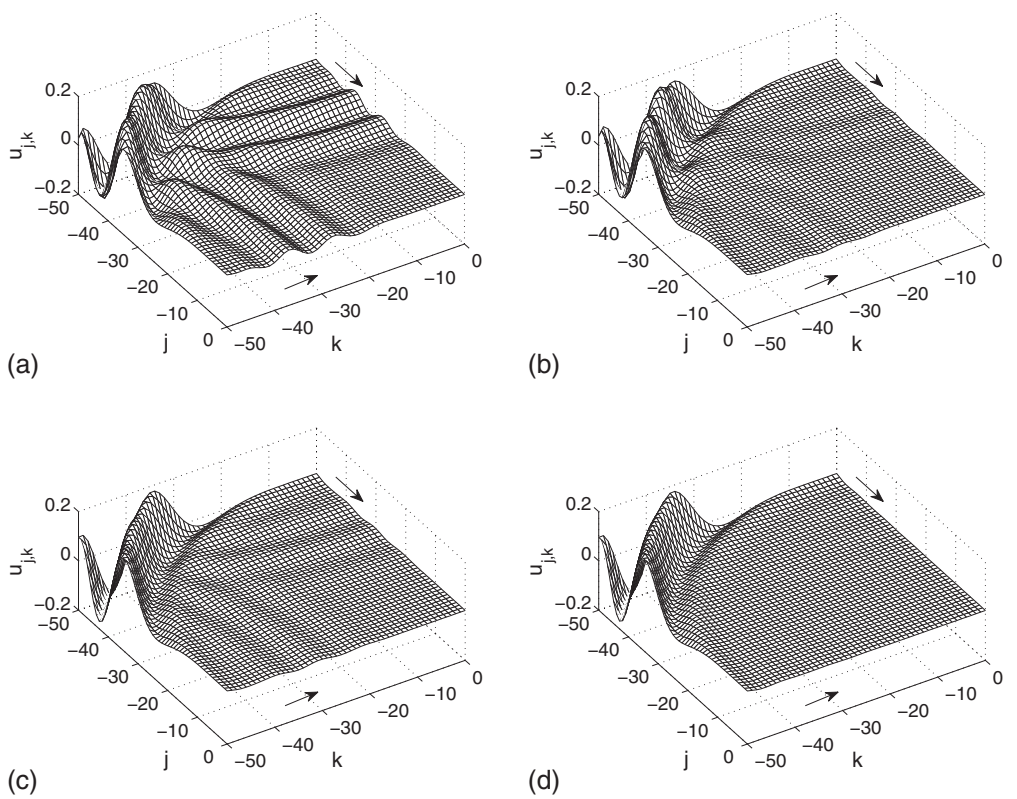

Figure 17. Displacement at $t = 70$ with (a) VIC1, (b) MBC1, (c) V1V1, and (d) M1M1. The test is with $\xi_0 = 0.5$. Because of the symmetry, only a quarter of the computing domain is shown. Arrows illustrate the propagation directions of reflection waves.

DOI: 10.1002/nme

For the test with $\xi_0 = 1$, we compare the numerical solutions at $t = 80$ shown in Figure 18. We observe again that MBC1 is much more effective than VIC1, and the operator multiplication significantly improves reflection suppression.

To quantify the reflection, we define the total energy in the computed patch.

$$E(t) = \frac{1}{2}\sum_{j=-50}^{49}\sum_{k=-49}^{49}(u_{j+1,k}-u_{j,k})^2 + \frac{1}{2}\sum_{j=-49}^{49}\sum_{k=-50}^{49}(u_{j,k+1}-u_{j,k})^2 + \frac{1}{2}\sum_{j=-50}^{50}\sum_{k=-50}^{50}\dot{u}_{j,k}^2.$$

The energy evolution, rescaled by the initial energy $E_0 = E(0)$, is plotted in Figure 19. Even in these two tests with short waves dominating, the reflection energy induced by MBC1 is at the magnitude of 10^{-3}, close to that with V1V1. M1M1 and M1M1M1 induce much smaller reflections.

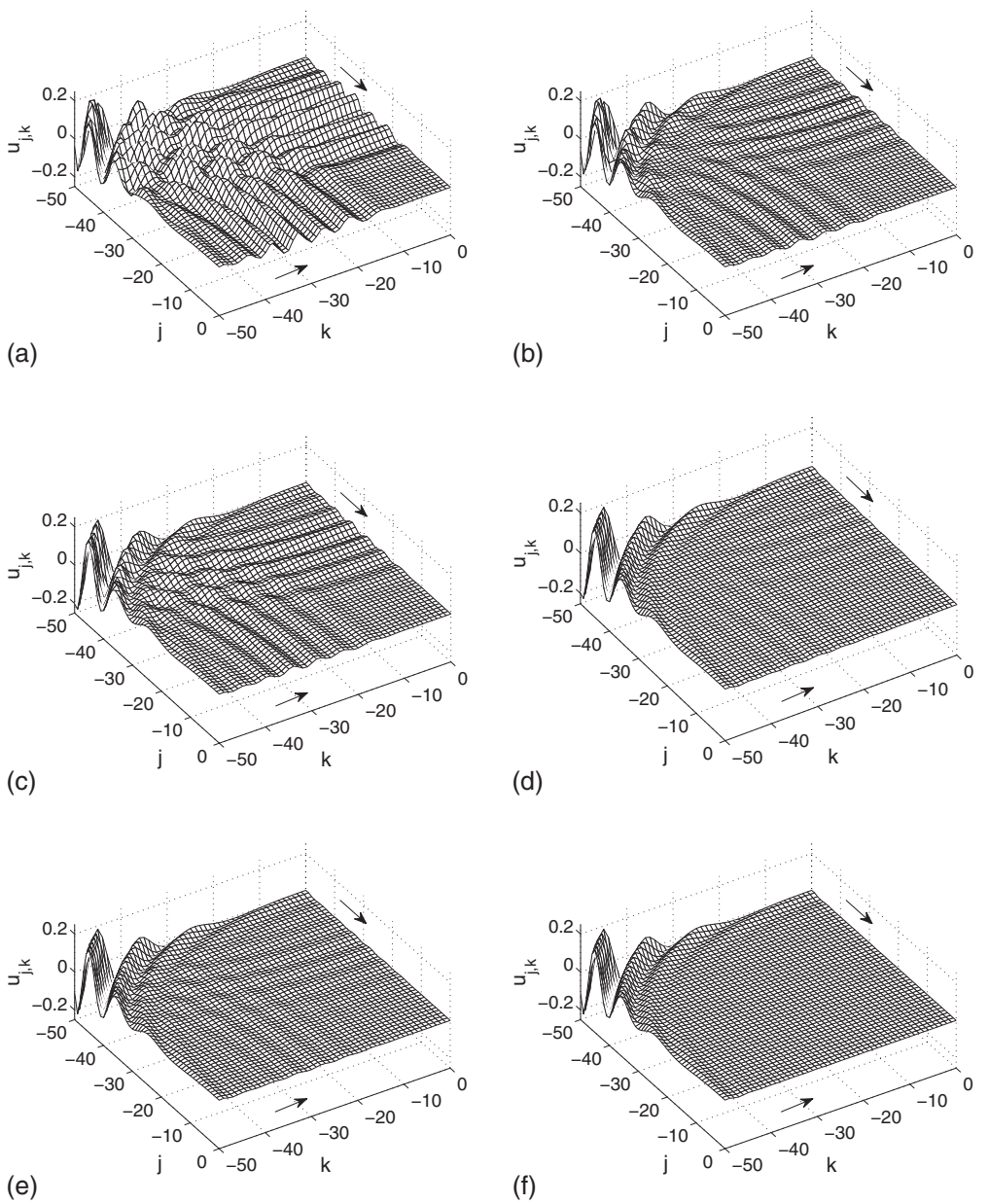

Figure 18. Displacement at $t = 80$ with (a) VIC1, (b) MBC1, (c) V1V1, (d) M1M1, (e) V1V1V1, and (f) M1M1M1. The test is with $\xi_0 = 1$. Because of the symmetry, only a quarter of the computing domain is shown. Arrows illustrate the propagation directions of reflection waves.

DOI: 10.1002/nme

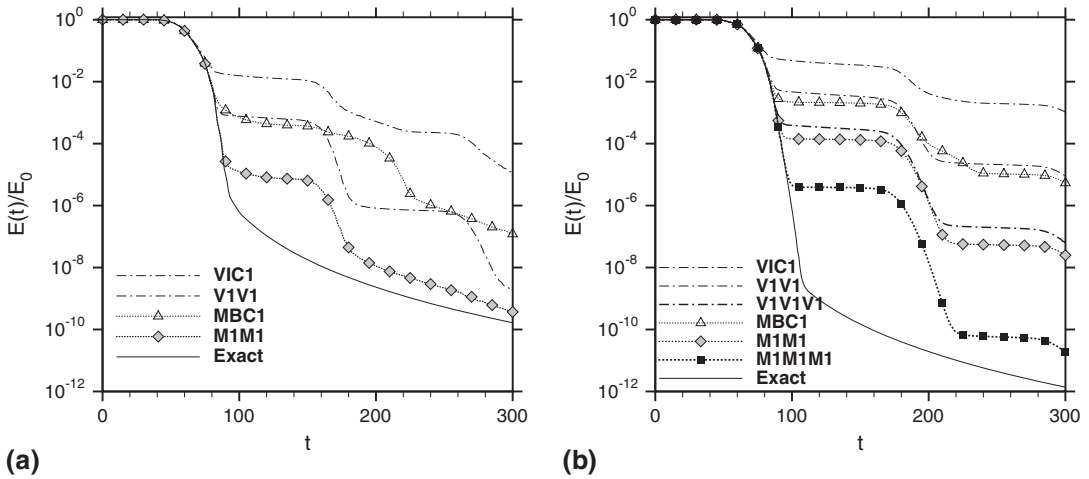

Figure 19. Energy evolution on the patch in the tests with (a) $\xi_0 = 0.5$ and (b) $\xi_0 = 1$.

In summary, we demonstrate the effectiveness of the proposed MBCs. MBC1 is more effective than VIC1 as the operator factor ABC in the design of multidirectional ABCs. This is consistent with the reflection coefficient analysis. In these two tests, wave lengths are fairly small. For most applications, we recommend M1M1 for the boundary treatment to suppress reflections.

6. NONLINEAR LATTICES AND MULTISCALE EXAMPLES

In this section, we adopt MBCs as boundary conditions for nonlinear lattices and apply them in multiscale simulations.

The locality and the simplicity for construction make MBCs directly applicable to multiscale computations of nonlinear lattices, similar to the VICs [16]. Compared with the time history kernel treatment, MBCs are much easier to implement.

6.1. One space dimension

Consider a nonlinear chain with nearest neighboring interactions governed by

$$\ddot{u}_j = f_j(u_{j+1} - u_j, u_{j-1} - u_j). \tag{56}$$

We first locally linearize the chain near the left boundary (the 0th atom)

$$\ddot{u}_j = C_L^2(t)(u_{j+1} - 2u_j + u_{j-1}), \;\; C_L(t) = \sqrt{f_1/(u_0 - 2u_1 + u_2)}. \tag{57}$$

Then, the MBC reads

$$\sum_{j=0}^{N} c_j \dot{u}_j = C_L(t) \sum_{j=0}^{N} b_j u_j. \tag{58}$$

6.1.1. Anharmonic chain. We use MBCs as ABCs for an anharmonic chain with a parameter $\bar{K}$ characterizing the cubic nonlinearity. In this chain, the interaction force acting on the jth atom is

$$f_j = (u_{j+1} - 2u_j + u_{j-1}) + \bar{K}\left[(u_{j+1} - u_j)^3 - (u_j - u_{j-1})^3\right]. \tag{59}$$

We consider a segment of 201 atoms of the infinite chain, numbered from -100 to 100. Numerical integrations are performed in the same way as the linear chain.

The numerical results for initial data

$$u_j(0) = \begin{cases} 2e^{-j^2/100}, & |j| < 70, \\ 0, & \text{elsewhere}, \end{cases} \qquad \dot{u}_j(0) = 0, \tag{60}$$

DOI: 10.1002/nme

are shown in Figure 20. In this test, the maximal local deformation is over 8%. Numerical solutions at $t = 150$ with the cubic nonlinearity parameter $\bar{K} = 5$ and 10 are displayed in the subplots (a) and (b), respectively. We observe that MBC1 produces much more accurate solution than the other two boundary treatments. In contrast, the least compact condition sVIC2 performs worst for increasing nonlinearity. We remark that at $\bar{K} = 10$, the exact solution is not zero at $t = 150$, resulted from the strong nonlinearity.

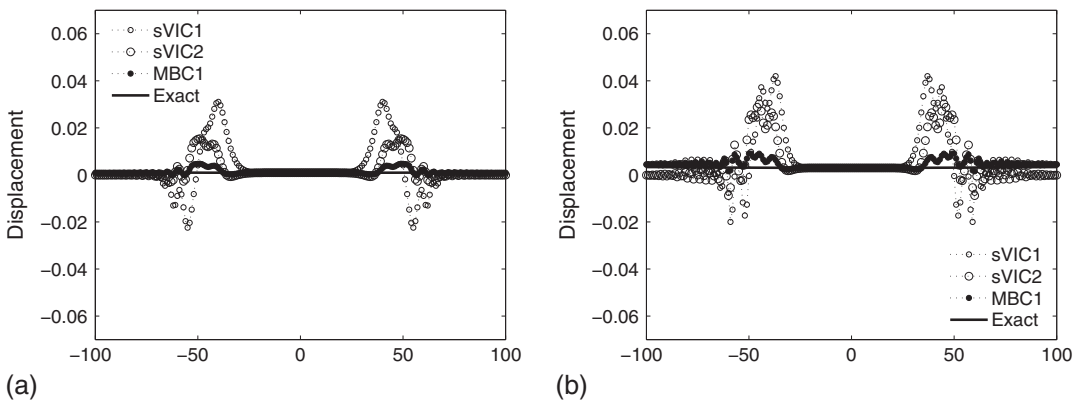

Figure 20. Numerical solutions with sVIC1, sVIC2, and MBC1 at $t = 150$: (a) $\overline{K} = 5$; (b) $\overline{K} = 10$. The horizontal axes denote the atom numbering.

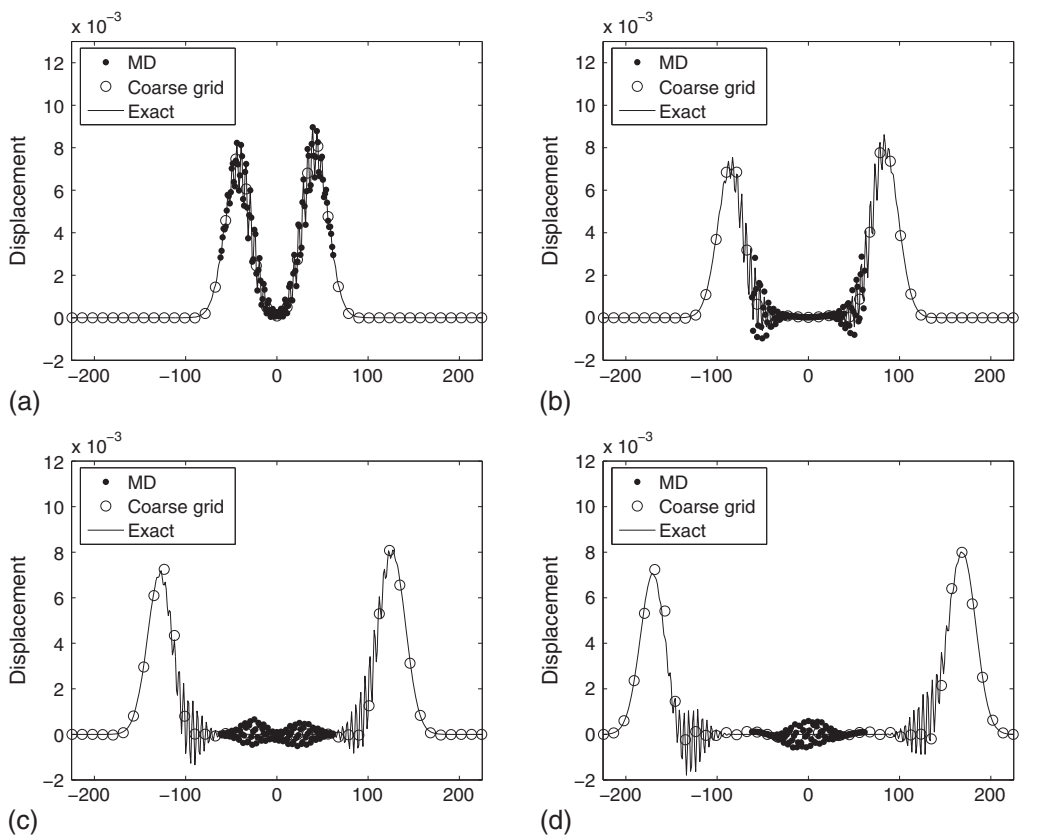

Figure 21. Multiscale test with sVIC1 at (a) $t = 5$, (b) $t = 10$, (c) $t = 15$, and (d) $t = 20$. The horizontal axes denote the atom positions at rest.

DOI: 10.1002/nme

6.1.2. Multiscale simulation of a chain with Lennard–Jones potential. We use MBCs to treat the numerical interfaces in a multiscale computation under the framework of the finite difference approach [16].

For the chain with the Lennard–Jones potential, the force term is [16]

$$f_j = 24\left[(r_0 + u_{j+1} - u_j)^{-7} - (r_0 + u_j - u_{j-1})^{-7}\right] - 48\left[(r_0 + u_{j+1} - u_j)^{-13} - (r_0 + u_j - u_{j-1})^{-13}\right]. \tag{61}$$

Here, $r_0 = 2^{1/6}$ is the atomic spacing at rest.

The coarse scale displacement d_J is updated with [16],

$$\begin{aligned}\ddot{d}_J =& -\frac{48}{p}\left[\left(r_0 + \frac{d_{J+1} - d_J}{p}\right)^{-13} - \left(r_0 + \frac{d_J - d_{J-1}}{p}\right)^{-13}\right] \\ &+ \frac{24}{p}\left[\left(r_0 + \frac{d_{J+1} - d_J}{p}\right)^{-7} - \left(r_0 + \frac{d_J - d_{J-1}}{p}\right)^{-7}\right] \\ &+ \frac{(p^2-1)\left(-52r_0^{-14} + 14r_0^{-8}\right)}{p^4}\left(d_{J-2} - 4d_{J-1} + 6d_J - 4d_{J+1} + d_{J+2}\right).\end{aligned} \tag{62}$$

The coarsening ratio is chosen as $p = 10$.

We compute for two sets of initial profiles in the whole domain $\Omega = [-200r_0, 200r_0]$ with 41 coarse grid points and the MD domain $\Omega_D = [-55r_0, 55r_0]$. For the fine and coarse scales, the time integration of the dynamics is performed with time step sizes $\Delta\tau = 0.001$ and $\Delta t = 0.01$, respectively.

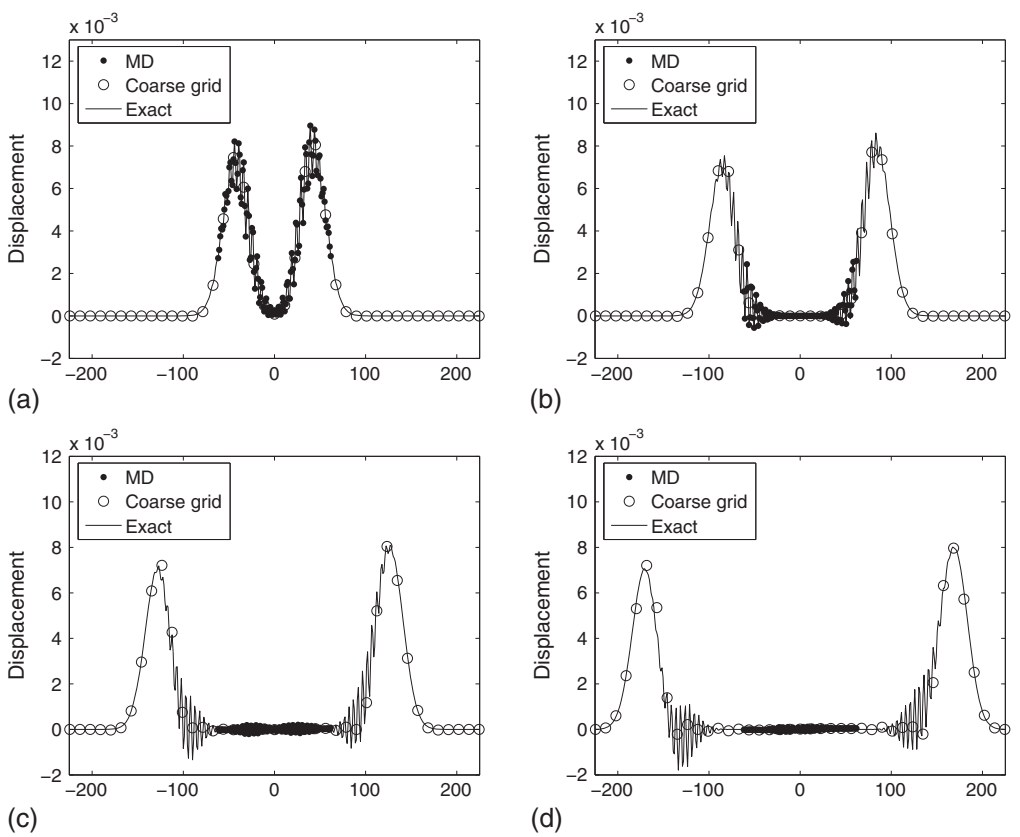

Figure 22. Multiscale test with MBC1 at (a) $t = 5$, (b) $t = 10$, (c) $t = 15$, and (d) $t = 20$. The horizontal axes denote the atom positions at rest.

DOI: 10.1002/nme

The numerical results for initial data

$$u_j(0) = \begin{cases} 0.015\frac{e^{-(jr_0/20)^2}-e^{-25}}{1-e^{-25}}[1+0.2\cos(2\pi jr_0/5)], & |jr_0|<100, \\ 0, & \text{elsewhere}, \end{cases} \qquad \dot{u}_j(0)=0, \quad (63)$$

with the interfacial conditions sVIC1, MBC1, and MBC2 are depicted in Figures 21–23, respectively. The multiscale computations with MBCs agree with the full MD solution very well, and all the coarse grid solutions catch the main waves. As mentioned previously, sVIC1 does not well absorb short waves. The corresponding multiscale solution differs from the full atomic computation with considerable wave reflection in the MD domain at $t = 15$ and $t = 20$ (Figure 21). In contrast, MBC1 suppresses the reflection effectively, and MBC2 further improves.

For an initial profile with larger deformation, the nonlinearity increases. For instance, we compute with

$$u_j(0) = \begin{cases} 0.15\frac{e^{-(jr_0/20)^2}-e^{-25}}{1-e^{-25}}[1+0.1\cos(2\pi jr_0/5)], & |jr_0|<100, \\ 0, & \text{elsewhere}, \end{cases} \qquad \dot{u}_j(0)=0. \quad (64)$$

The numerical results with MBC2 in Figure 24 still agree well with the exact solution. We remark that linear elasticity usually requires a strain below 1%. In this test, the local deformation is over 5%.

We observe that MBC2 performs much better than mVIC4. We remark that mVIC4 had been shown to be more efficient than the time history kernel treatment, which is used in the bridging scale method. See Figures 16 and 18 in [16]. To our knowledge, the compact MBCs are the most efficient in this setting of multiscale simulations for nonlinear lattices.

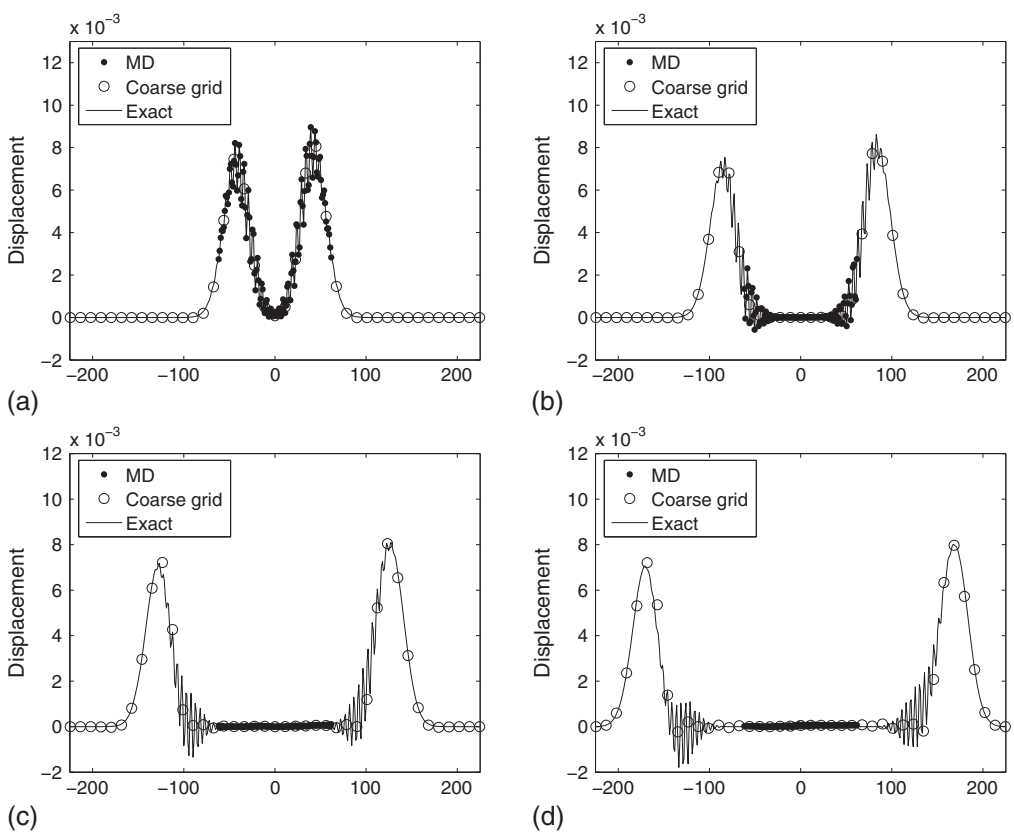

Figure 23. Multiscale test with MBC2 at (a) $t = 5$, (b) $t = 10$, (c) $t = 15$, and (d) $t = 20$. The horizontal axes denote the atom positions at rest.

DOI: 10.1002/nme

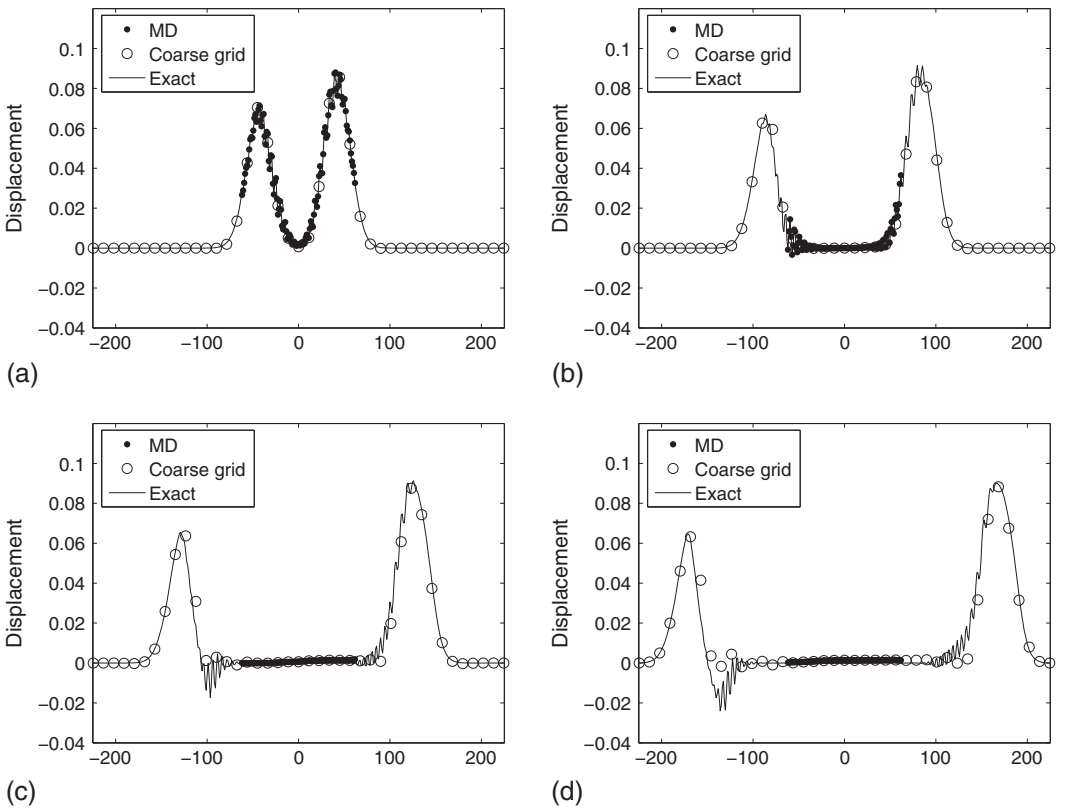

Figure 24. Multiscale test under a larger deformation with MBC2 at (a) $t = 5$, (b) $t = 10$, (c) $t = 15$, and (d) $t = 20$. The horizontal axes denote the atom positions at rest.

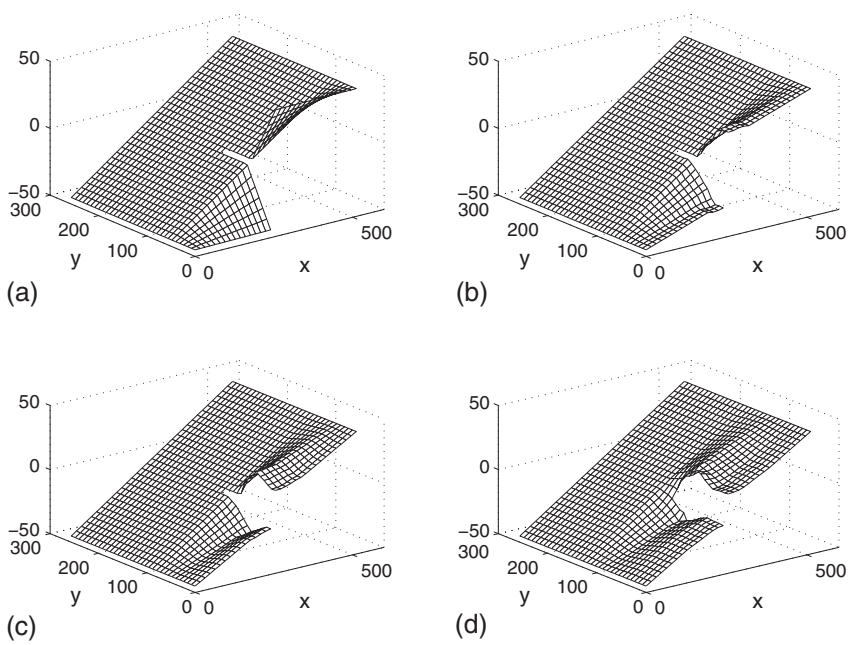

Figure 25. Coarse grid displacement in Slepyan model by the multiscale simulation at (a) $t = 0$, (b) $t = 20$, (c) $t = 40$, and (d) $t = 80$.

DOI: 10.1002/nme

6.2. Two space dimensions: multiscale simulation of Mode III fracture

We apply MBC1 to treat the atomic-coarse grid interfaces in a multiscale computation of Mode III fracture by the Slepyan model [31]. The multiscale computation is under the framework of the finite difference approach [16]. For the sake of convenience, we take the dimensionless atomic spacing $h_a = 1$.

A Slepyan model describes dynamic Mode III fracture in a square lattice [31]. The displacement out of the lattice plane $u_{j,k}$ is governed by

$$\ddot{u}_{j,k} = -b\dot{u}_{j,k} + \sum_{j'k'} (u_{j',k'} - u_{j,k})\Theta(2 - |u_{j',k'} - u_{j,k}|). \tag{65}$$

Here, Θ denotes the Heaviside step function, and $b = 0.01$ is the damping coefficient. In multiscale computations, the MD simulation subdomain is allocated so that the artificial interfaces between this subdomain and coarse grid are away from the crack, where the model is harmonic and the same as the square lattice discussed previously. Therefore, the MBCs can be easily implemented.

We perform a multiscale simulation over a domain including 513×257 atoms. The initial profile contains a crack between the 256th and 257th layers in the x-direction, from the first atom to the 48th in the y-direction. We take the atomic subdomain $\Omega_A = [178, 335] \times [1, 257]$ and update the coarse grid displacement $d_{J,K}$'s by [16]

$$\begin{aligned} \ddot{d}_{J,K} = {} & \frac{1}{p_x^2}(d_{J-1,K} - 2d_{J,K} + d_{J+1,K}) + \frac{1}{p_y^2}(d_{J,K-1} - 2d_{J,K} + d_{J,K+1}) \\ & + \frac{p_x^2 - 1}{12p_x^4}(d_{J-2,K} - 4d_{J-1,K} + 6d_{J,K} - 4d_{J+1,K} + d_{J+2,K}) \\ & + \frac{p_y^2 - 1}{12p_y^4}(d_{J,K-2} - 4d_{J,K-1} + 6d_{J,K} - 4d_{J,K-1} + d_{J,K-2}) - b\dot{d}_{J,K} \end{aligned} \tag{66}$$

with the coarsening ratios $p_x = p_y = 8$. For the atomic and the coarse scales, the time integration of the dynamics is performed with the speed Verlet scheme at time step sizes $\Delta\tau = 0.05$ and $\Delta t = 0.5$, respectively.

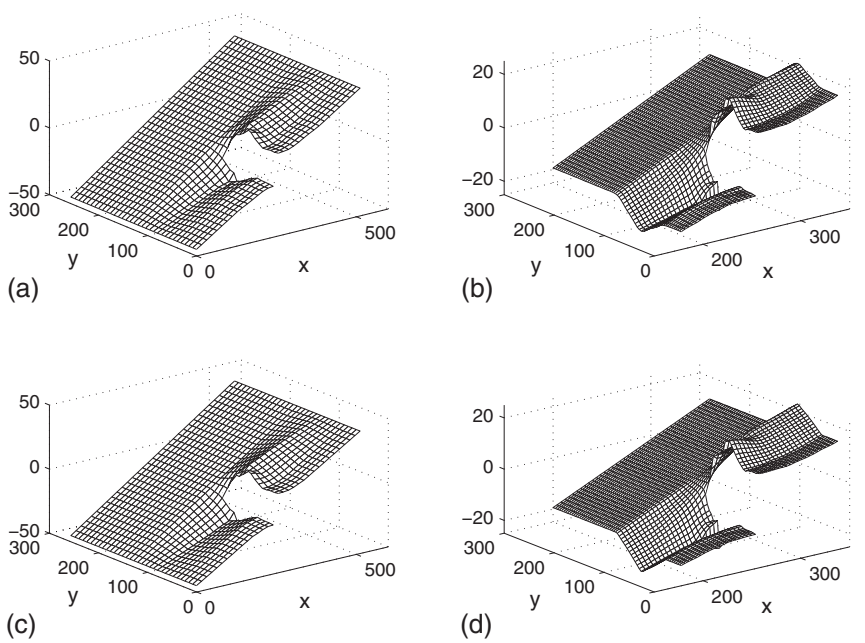

Figure 26. Displacement in Slepyan model at $t = 80$: (a) coarse grid solution by the multiscale computation, (b) MD solution in Ω_A by the multiscale computation, (c) the full MD solution, and (d) the full MD solution in Ω_A.

DOI: 10.1002/nme

The coarse grid displacement evolution of the multiscale computation is shown in Figure 25. The crack propagates along the y-direction. As shown in Figure 26, the multiscale computation agrees well with the full MD solution at $t = 80$. Differences in displacements are almost indiscernible, both at the coarse grid level and in the atomic subdomain. With such a thin strip for the atomic subdomain, the multiscale method with MBC1 gives an accurate resolution for the fracture. More detailed computations show that MBC1 performs better than the computationally more expensive time history treatment that has been used in the bridging scale method [16].

7. CONCLUSION

In this paper, we develop a new class of accurate and efficient ABCs to suppress spurious reflections at MD artificial boundaries for simulations of crystalline solids.

For one-dimensional chains, the proposed MBCs take the form of a linear combination of displacement and velocity at atoms near the artificial boundary, with the coefficients determined by matching the dispersion relation of the lattice vibrations. Perfect absorption may be reached for the outgoing waves at selected wave numbers. Reflection suppression is enhanced progressively by involving more neighboring atoms in the conditions. In particular, high accuracy can be reached in the long wave limit.

Extensions to multiple dimensional lattices, specifically, MBCs for the out-of-plane wave propagation in the square lattice are further proposed. Similar to the one-dimensional cases, by matching the dispersion relation, we design MBCs perfectly absorbing normal incidence in the long wave limit. Each unidirectional MBC treats plane waves in a certain incident direction effectively. Then, we design multidirectional MBCs by using the products of these MBC operators. The operator multiplication MBCs further reduce reflection effectively. Moreover, they involve only a small number of atoms, thanks to the compactness of the one-dimensional MBCs. Meanwhile, all of them can be recast into the displacement–velocity form.

The effectiveness of the proposed MBCs is demonstrated by the reflection coefficient analysis and numerical tests. Comparisons are made with other treatments, such as the time history kernel treatment and the VICs. The proposed MBCs are demonstrated to be more efficient.

To our best knowledge of the state of the art, it is the first time to propose the general displacement–velocity form of ABCs, to design them by matching the dispersion relation directly, and to construct multidirectional conditions based on such kind of ABCs. The effectiveness of an operator multiplication ABC depends on the effectiveness of the corresponding operator factor ABCs. For instance, the multidirectional ABCs based on MBC1 are more effective than those based on VIC1. We remark that the Higdon ABCs designed for continuous waves has been applied to discrete lattices [36]. Careful comparison shows that they are less effective to suppress reflections than MBCs.

In conclusion, the proposed MBCs are effective as ABCs for MD simulations and multiscale simulations of crystalline solids. They reach high efficiency, namely excellent reflection suppression at the cost of negligible computing load. Furthermore, the spatial and temporal localities allow a direct and effective application to nonlinear lattices, similar to the VICs but with higher accuracy. For most applications, MBCs with a few atoms near the boundary suffice for the accuracy requirements. The implementation and extensions to other lattices are straightforward. For instance, local ABCs for diatomic chains have been proposed, which treat simultaneously the acoustic and optical phonons effectively [35]. In forthcoming papers, MBCs are extended to the wave propagation in the triangular lattice [37] and some three dimensional lattices [38, 39].

APPENDIX A. VELOCITY INTERFACIAL CONDITIONS AND DEGENERATE MATCHING BOUNDARY CONDITIONS

Some existing boundary conditions can be viewed as special cases of the proposed displacement–velocity form (3), but they are less compact than the proposed MBCs in this paper. Typical conditions include the VIC [16] and the force boundary condition [35].

DOI: 10.1002/nme

For the one-dimensional harmonic chain (2), a single-layer VIC (sVIC for short) takes the form of

$$\dot{u}_0 = \sum_{j=0}^{N} b_j u_j, \tag{A.1}$$

where the coefficients b_j's can be determined by matching the dispersion relation at $\xi = 0$ in the same way as MBCs. For instance, the simplest two conditions are

$$\dot{u}_0 = -u_0 + u_1, \;\; \dot{u}_0 = -\frac{3}{2}u_0 + 2u_1 - \frac{1}{2}u_2,$$

named sVIC1 and sVIC2, respectively.

As an improvement, multilayer VICs (mVICs for short) were derived [16]. In that treatment, evolutions of several layers of atoms near the boundary are constructed in the similar way. For instance, the second-order multilayer VIC (mVIC2 for short) is

$$\begin{cases} \dot{u}_0 = -\frac{3}{2}u_0 + 2u_1 - \frac{1}{2}u_2, \\ \dot{u}_1 = -\frac{1}{2}u_0 + 0u_1 + \frac{1}{2}u_2. \end{cases} \tag{A.2}$$

It is equivalent to the following single-layer condition.

$$\ddot{u}_1 = -u_1 + u_2 - \frac{3}{2}\dot{u}_1 + \frac{1}{2}\dot{u}_2. \tag{A.3}$$

Moreover, using the Newton equation $\ddot{u}_1 = u_0 - 2u_1 + u_2$, we have

$$u_0 - u_1 = -\frac{3}{2}\dot{u}_1 + \frac{1}{2}\dot{u}_2. \tag{A.4}$$

This falls into the category of our linear displacement–velocity form as well. The situations of higher order mVICs are similar.

Given $c_0 = 0$ and $b_0 = 1$, (3) directly gives the displacement u_0, that is,

$$u_0 = \sum_{j=1}^{N} c_j \dot{u}_j - \sum_{j=1}^{N} b_j u_j. \tag{A.5}$$

The coefficients in (A.5) can be determined by solving linear equation systems similar to (10) or (18) without the highest order equation of ξ in the long wave limit. The degenerate MBC (A.5) is equivalent to a force boundary condition at the 1st atom, which has been designed and used for diatomic chains [35].

In summary, the displacement–velocity form (3) is quite general. In fact, because higher order derivatives in time can be reduced into displacement or velocity by using the Newton equations, all linear conditions of these kinds can be transformed into the form (3). Furthermore, the MBCs proposed in this paper is the most compact ones.

ACKNOWLEDGEMENTS

We would like to thank the anonymous reviewers for stimulating discussions. This research is partially supported by NSFC under contract number 11272009 and the National Basic Research Program of China under contract number 2010CB731503.

REFERENCES

1. Liu WK, Karpov EG, Park HS. *Nano Mechanics and Materials: Theory, Multiscale Methods and Applications*. Wiley: New York, 2005.
2. Fish J. Bridging the scales in nano engineering and science. *Journal of Nanoparticle Research* 2006; **8**:577–594.

DOI: 10.1002/nme

3. Miller RE, Tadmor EB. Hybrid continuum mechanics and atomistic methods for simulating materials deformation and failure. *MRS Bulletin* 2007; **32**:920–926.
4. Li X. On the stability of boundary conditions for molecular dynamics. *Journal of Computational and Applied Mathematics* 2009; **231**:493–505.
5. Adelman SA, Doll JD. Generalized Langevin equation approach for atom/solid-surface scattering: collinear atom/harmonic chain model. *Journal of Chemical Physics* 1974; **61**:4242–4245.
6. Cai W, de Koning M, Bulatov VV, Yip S. Minimizing boundary reflections in coupled-domain simulations. *Physical Review Letters* 2000; **85**:3213–3216.
7. Wagner GJ, Liu WK. Coupling of atomistic and continuum simulations using a bridging scale decomposition. *Journal of Computational Physics* 2003; **190**:249–274.
8. Karpov EG, Wagner GJ, Liu WK. A Green's function approach to deriving nonreflecting boundary conditions in molecular dynamics simulations. *International Journal for Numerical Methods in Engineering* 2005; **62**: 1250–1262.
9. Liu WK, Karpov EG, Zhang S, Park HS. An introduction to computational nano mechanics and materials. *Computer Methods in Applied Mechanics and Engineering* 2004; **193**:1529–1578.
10. Park HS, Karpov EG, Klein PA, Liu WK. Three-dimensional bridging scale analysis of dynamic fracture. *Journal of Computational Physics* 2005; **207**:588–609.
11. Park HS, Karpov EG, Liu WK, Klein PA. The bridging scale for two-dimensional atomistic/continuum coupling. *Philosophical Magazine* 2005; **85**:79–113.
12. Tang S, Hou TY, Liu WK. A mathematical framework of the bridging scale method. *International Journal for Numerical Methods in Engineering* 2006; **65**:1688–1713.
13. Tang S, Hou TY, Liu WK. A pseudo-spectral multiscale method: interfacial conditions and coarse grid equations. *Journal of Computational Physics* 2006; **213**:57–85.
14. Liu WK, Qian D, Gonella S, Li SF, Chen W, Chirputkar S. Multiscale methods for mechanical science of complex materials: bridging from quantum to stochastic multiresolution continuum. *International Journal for Numerical Methods in Engineering* 2010; **83**:1039–1080.
15. Pang G, Tang S. Time history kernel functions for square lattice. *Computational Mechanics* 2011; **48**:699–711.
16. Tang S. A finite difference approach with velocity interfacial conditions for multiscale computations of crystalline solids. *Journal of Computational Physics* 2008; **227**:4038–4062.
17. Engquist B, Majda A. Radiation boundary conditions for acoustic and elastic calculations. *Communications on Pure and Applied Mathematics* 1979; **32**:313–357.
18. E W, Huang Z. Matching conditions in atomistic-continuum modeling of materials. *Physical Review Letters* 2001; **87**:135501.
19. Li X, E W. Variational boundary conditions for molecular dynamics simulation of solids at low temperature. *Communications in Computational Physics* 2006; **1**:135–175.
20. Jones RE, Kimmer CJ. Efficient non-reflecting boundary condition constructed via optimization of damped layers. *Physical Review B* 2010; **81**:094301.
21. Fang M, Tang S. Efficient and robust design for absorbing boundary conditions in atomistic computations. *Chinese Physics Letters* 2009; **26**:116201.
22. Berenger JP. A perfectly matched layer for the absorption of electromagnetic waves. *Journal of Computational Physics* 1994; **114**:185–200.
23. Clayton R, Engquist B. Absorbing boundary conditions for acoustic and elastic wave equations. *Bulletin of the Seismological Society of America* 1977; **67**:1529–1540.
24. Feng K. Asymptotic radiation conditions for reduced wave equation. *Journal of Computational Mathematics* 1984; **2**:130–138.
25. Keller JB, Givoli D. Exact non-reflecting boundary conditions. *Journal of Computational Physics* 1989; **82**: 172–192.
26. Higdon RL. Absorbing boundary conditions for the wave equation. *Mathematics of Computation* 1987; **49**:65–90.
27. To AC, Li S. Perfectly matched multiscale simulations. *Physical Review B* 2005; **72**:035414.
28. Li S, Liu X, Agrawal A, To AC. Perfectly matched multiscale simulations for discrete lattice systemsExtension to multiple dimensions. *Physical Review B* 2006; **74**:045–418.
29. Guddati MN, Thirunavukkarasu S. Phonon absorbing boundary conditions for molecular dynamics. *Journal of Computational Physics* 2009; **228**:8112–8134.
30. Carpio A, Tapiador B. Nonreflecting boundary conditions for discrete waves. *Journal of Computational Physics* 2010; **229**:1879–1896.
31. Slepyan LI, Ayzenberg-Stepanenko MV, Dempsey JP. A lattice model for viscoelastic fracture. *Mechanics of Time-Dependent Materials* 1999; **3**:159–203.
32. Brillouin L. *Wave Propagation in Periodic Structures: Electric Filters and Crystal Lattices*. McGraw-Hill: New York, 1946.
33. Born M, Huang K. *Dynamical Theory of Crystal Lattices*. Clarendon Press: Oxford, 1954.
34. Christman JR. *Fundamentals of Solid State Physics*. John Wiley & Sons Inc: New York, 1988.
35. Wang X, Tang S. Matching boundary conditions for diatomic chains. *Computational Mechanics* 2010; **46**: 813–826.

DOI: 10.1002/nme

36. Namilae S, Nicholson DM, Nukala PKVV, Gao CY, Osetsky YN, Keffer DJ. Absorbing boundary conditions for molecular dynamics and multiscale modeling. *Physical Review B* 2007; **76**:144111.
37. Wang X, Tang S. Matching boundary conditions for molecular dynamics simulations of triangular lattice. Preprint.
38. Fang M, Tang S, Li Z, Wang X. Artificial boundary conditions for atomic simulations of face-centered-cubic lattice. *Computational Mechanics*. DOI: 10.1007/s00466-012-0696-8. In press.
39. Fang M, Wang X, Li Z, Tang S. Matching boundary conditions for scalar waves in body-centered-cubic crystalline solids. Preprint.

DOI: 10.1002/nme